Master Thesis

ANALYSIS OF CHARGE BALANCER SYSTEM

An analysis of a charge equalizer system, and a battery and charge equalizer overview

MATTEO ZANIBELLATO

Faculty of Electrical and Information Engineering
University of Applied Sciences Regensburg

Prof.Dr. Manfred Bruckmann
Prof.Dr. Paolo Tenti

2012

A *Manuela* che ha sempre creduto in me.

Alla mia famiglia

Zum Adrian: er war immer da wenn ich ihn brauchte

Zu meine freunde Joseph und Martin, die die Bayerische kultur mir eingeführt haben

Fatti non foste a viver come bruti, ma per seguir virtute e canoscenza

— [Dante Alighieri]

Quelli che s'innamorano di pratica senza scienza
son come il nocchiere, che entra in naviglio senza bussola,
che mai ha certezza dove si vada

— [Leonardo da Vinci]

ACKNOWLEDGMENTS

Ich bedanke mich beim Herr Professor Manfred Bruckmann für diese gelegenheit

Ringrazio il Professore Paolo Tenti per avermi supportato

ABSTRACT

If the charge between batteries in a battery stack is not equalized, each battery will have a different stress due to their different conditions. Consequently, some of them are more stressed than others, decreasing the life-time of the entire battery pack. The here proposed topology has to ensure a fast and a high efficient charge transfer between each pair of cells. This work presents an overview about basic concepts of batteries, a general overview on charge equalizer systems, and a SPICE analysis of a peculiar bidirectional flyback used as charge equalizer. The mutual inductor is designed in order to reach the maximum efficiency.

SOMMARIO

Sistemi di accummulo dell'energia elettrica come UPSsono spesso costituiti da più batterie. A causa delle differenze elettro-chimiche intrinseche nelle batterie che compongono il pacco, ciascuna di queste presenta un diverso andamento: ciò comporta differenze nella carica elettrica immagazzinata. In conseguenza di ciò, dopo ripetuti cicli di carica/scarica le differenze si acuiscono sempre più, dando luogo a fenomeni di dendritizzazione che formano canali conduttivi interni alla batteria stessa e che vanno a cortocircuitare i poli. Al fine di evitare questa deriva, in letteratura sono stati presentati vari tipi di equalizzatori di carica "Charge Equalizer" che permettono di equalizzare la carica tra le batterie all'interno del pacco.

Nel seguente lavoro di tesi vengono presentati alcuni concetti di base sulle batterie al piombo oltre ad alcuni tra i modelli piu usati ed una panoramica delle tipologie di Charge Equalizer presenti in letteratura. Successivamente viene considerata l'ipotesi di applicare la topologia del convertitore Flyback come Charge Equalizer tra due batterie, l'unica carica al 70%, l'altra al 30%. Tale topologia viene utilizzata sia per fornire un isolamento galvanico alle due batterie, che per la sua possibilità di funzionare da Buck-Boost. Particolare attenzione è stata posta nel dimensionare il mutuo induttore al fine di minimizzare le perdite di energia trasferita da una batteria all'altra. Infine il circuito viene dimensionato utilizzando un doppio anello di retroazione sia di corrente (inerno), che di tensione. Tale convertitore deve infatti fornire corrente costante alla batteria meno carica finchè le tensioni delle due batterie raggiungono il medesimo livello. L'anello di tensione utilizza come riferimento la tensione della batteria più carica, ed il regolatore processa la differenza tra questa e la tensione della batteria meno carica.

In tal modo si intende fornire un'analisi attraverso la simulazione di questo tipo di Charge Equalizer in LTSpice, che permetta la sua realizzazione.

1

BASICS OF BATTERIES

A battery is an electrochemical device made up of one or more buildings blocks, or cells (Voltaic cells). Galvanic or voltaic cells consist of two dissimilar electrodes (one positive and one negative) immersed in a conducting material such as a liquid electrolyte or a fused salt and a porous separation between the electrodes. At the separation surface between the metal and the solution there exists a difference in electrical potential, called *electrode potential*. The electromotive force (e.m.f.) is then equal to the algebraic sum of potential electrodes that compose the cell. When a metal is placed in a liquid, there is in general a potential difference established between the metal and the solution owing to the metal yielding ions to the solution (negatively charged) or the solution yielding ions to the metal (positively charged). Since the total e.m.f. of a cell can be calculated with the algebraic sum of the potential differences at two electrodes, it follows that the total e.m.f. of the battery is equal to the algebraic sum of potential differences of each cell composing battery [2]. During the charging or discharging

Galvanic cell

Cell e.m.f.

Battery e.m.f.

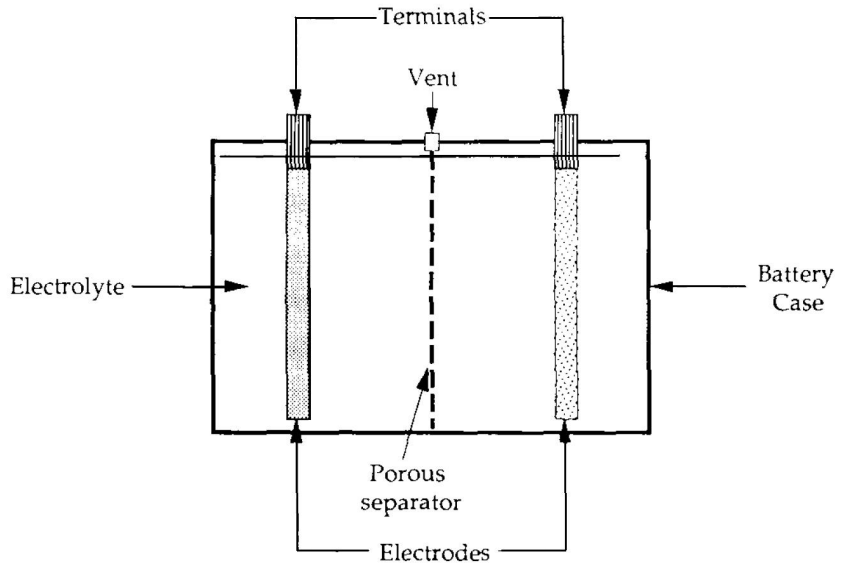

Figure 1: Conceptual diagram of an electrochemical battery cell [13]

phase, the electrodes undergo an oxidation-reduction (redox) reaction, which effects the transfer of ions to and/or from electrodes. The flow of ions manifests the charge flow that appears as battery current. A higher rate of charge transfer implies a need for greater exposure of electrode surface area to the electrolyte. In order to achieve this aim, a high porosity on the electrode surface area is required. A high rate of charge transfer also implies a need for shorter electrode-to-electrode distance for ion travel. Battery electrodes are consequently often fabricated as a set of closely interleaved plates.

1.0.1 *Battery Capacity*

Battery capacity is measured in Amp-hour, and is defined as the stored charge, that can be delivered to a constant current load up to a pre-defined cut-off voltage [8].

$$C = \int_{\Delta t} i dt \tag{1.1}$$

In normal conditions cell's capacity is almost constant: just in the end of battery life falls below 80%. Cells and batteries are rated at standard specified values of discharge rates and other application conditions. Rated capacity (C) for each cell or battery is defined as the minimum standard capacity to be expected from any example of that type when new, but fully formed and stabilized. The rated value must also be accompanied by the hour-rate of discharge. (figure of the cell selector guide Pg259 [1])

1.0.2 *Battery modeling*

To model a lead-acid battery using the available data provided by manufacturers, algebraic equations can be used. The dynamic model uses the manufacturers' data combined with algebraic equations. Battery capacity can be described by a function of discharge current (Peukert's Equation), and discharge voltage as a function of SOC; battery internal resistance as a function of SOC (State Of Charge). [[8] this article presents a rechargeable lead-acid battery, Yuasa DM55-12, 12V, 57Ah that was modeled using manufacturers' data sheet parameters and selected handbook curves]

Peukert's Equation

Cell capacity is strictly related with the discharge current I_d. In 1897 Peukert determined the cell capacity as:

$$C = \frac{K}{I_d{}^{(p-1)}} \tag{1.2}$$

where K and p are provided by manufactures (and typically p is between 1.3 and 1.4). Figure 2 represents the battery capacity as a function of discharge current for 3 A to 500 A.

The resulting curve in figure:2 is also used to generate the Peukert's equation

Discharge Voltage

The battery terminal voltage (end-point voltage) is a function of the state of charge of the battery. An example of discharge profile curve is showed in figure: 3 (a typical discharge profile curve can be found in [1], pp 166-175]).

Figure 4 shows the typical discharge profile and the algebraic equations pointing out the complex relationship between the cell voltage and SOC.

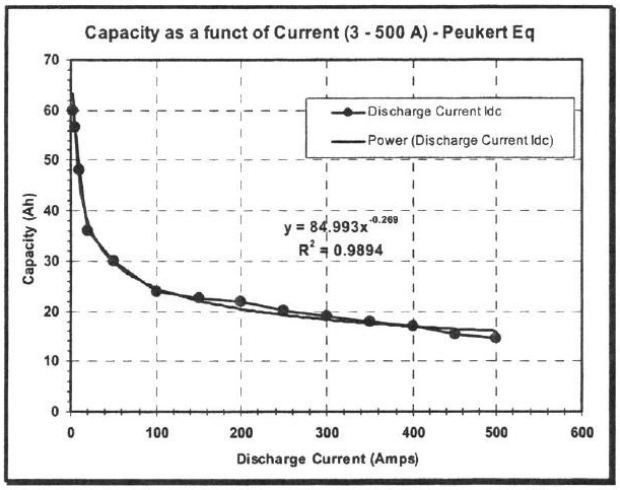

Figure 2: Capacity versus discharge current for 3A to 500A as computed from manufacturer' reported from [8]

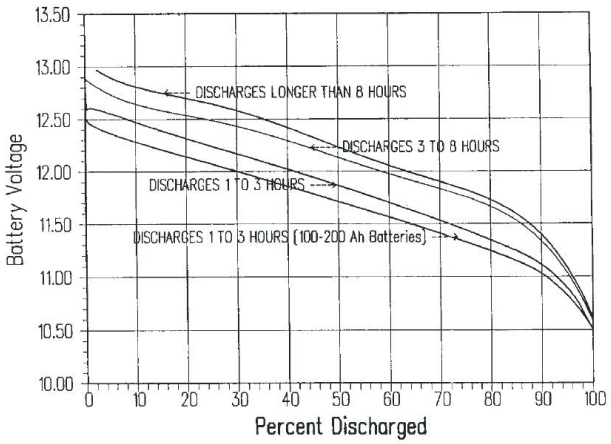

Figure 3: Battery voltage versus discharge percent [8]

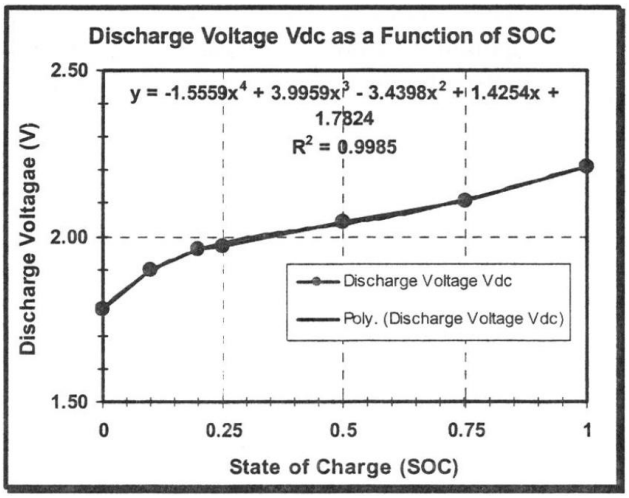

Figure 4: Voltage discharge versus SOC [8]

MID POINT VOLTAGE Mid point voltage is the voltage of the cell, when it delivered 50% of its capacity at the given discharge rate. It is also the approximated average voltage for the plateau of the discharge curve. This is a common way to estimate the discharge of a battery.

1.0.3 *Charging*

When the battery is charged, all the acid is driven out of the plates and has returned into the electrolyte, due to the direct current passed through the cell, in the opposite direction of the electrolyte flux in discharge phase. The concentration of the acid at the end of the charging-process is maximum [2] [18.1.2]. When the cell is fully charged, the active material of the positive plates is lead dioxide, and the active one of the negative part is metallic lead in spongy form. The concentration of acid in the electrolyte is at its maximum. The nominal voltage of a lead-acid cell is 2V, that it varies slightly depends slightly on the temperature, the charge or discharge current, and on the age of the cell.

VOLTAGE DURING CHARGE During charging phase there is an immediate rising in the battery voltage due to the sudden increase of the density of the electrolyte. The subsequent rise of voltage is governed by the rate at which the acid is produced in the plates and the rate of diffusion into the free electrolyte of the cell. When charging voltage on a single cell reaches 2.4V(see figure 5), there is a fairly sharp rise. At this stage it is full of lead sulfate. Most of the charge is used to dissociate sulfuric acid solution in hydrogen. When this happens the voltage increases; once this process is finished, the voltage does not rise any longher. Recharge is considered to be complete when the voltage and the relative density of the electrolyte remain constant for about 3 h [2].

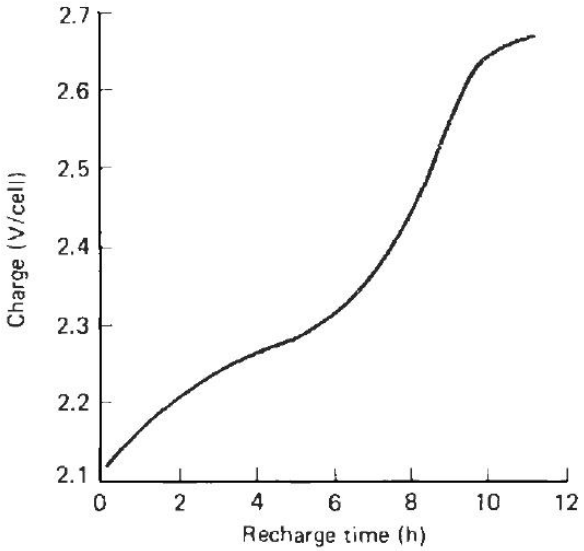

Figure 5: Variation of voltage of lead-acid cell during recharge ([2] pag18-3)

1.0.4 *Discharging*

When a battery is providing energy, it is said that the battery is discharging. The energy is provided by the acid in the electrolyte gradually, combined with the active material of the plates. This combination produces lead sulfate in both negative and positive plates. A cell is completely discharged when both plates are entirely sulfated (and are composed of identical material: at this point the voltage collapses, but in practice the discharge must be stopped long before the plates reached this stage) (see [2] 18.1.1- page 213).

Complete discharge

VOLTAGE DURING DISCHARGE The behaviour of the cell voltage during discharge is reverse to that on charge. The impedance of the cell creates a voltage drop when the discharge current is passing through, causing the voltage during discharge to be less than the voltage measured in the open circuit condition. (Voltage on discharge = Open circuit voltage - (Current x Internal resistance))

1.0.5 *Capacity*

The capacity of the battery varies according to the current during the discharging-phase. The higher the current being taken out of the battery, the lower the available capacity. For example, if a battery of 500Ah capacity is discharged at the 5h rate, it will give 100A for 5h; the same battery can also provide 200A, but only for 2h thereby providing a capacity of 400Ah at the 2h discharge. Indeed, at higher power rates, the voltage drop is more rapid and the final voltage is reached more quickly. Motive power battery capacities are normally given at the 5 or 6h rate of discharge. At low temperatures the capacity is considerably reduced The *relationship between capacity and discharge rate* is shown in figure 6 [[1]Pag.162 fig 4-3] is pointed out the relationship between capacity and the discharge rate.

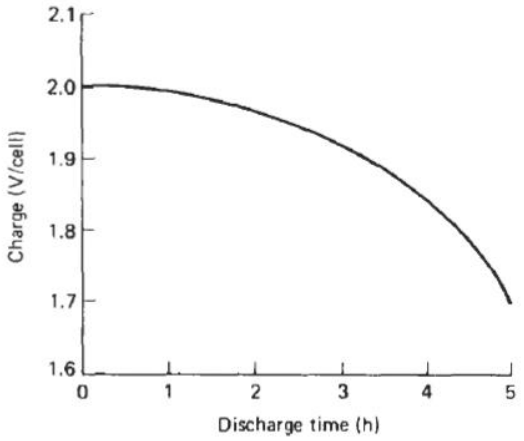

Figure 6: Variation of voltage of Lead-Acid Battery versus discharge time [2]

The classical method to plot discharge curve is to represent terminal voltage as function of discharge time, at a stipulated battery

temperature. It is common practice to state the available capacity at a particular discharge rate. Thus, if a battery is discharged continuously for 20h at 20°C, the nominal capacity is available, referred to as $1 \times C_{20}$ capacity. If instead, the same battery is continuosly discharged at a higher discharge current in 10h instead of 20h, the capacity is referred to as $2C_{20}$; that is:

$$\frac{20h}{10h} \times C_{20} = 2C$$

The higher the number in front of C_{20} is, the faster the process of the battery at the fixed temperature is. Vice versa, the smaller the number is, the slower the discharging process is.

Discharge rate (h)	*Approximate percentage of rated capacity*	*End-voltage* (V/cell)
20	100	1.75
10	97	1.70
5	88	1.65
1	62	1.50
0.5	52	1.00

Figure 7: The nominal capacity of a typical battery when discharged to various voltages as a percentage of its capacity for a single cell

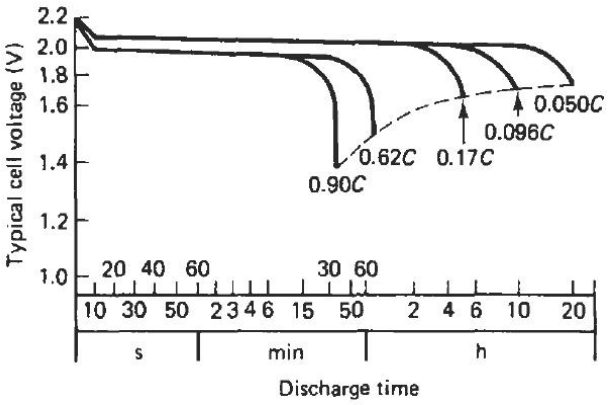

Figure 8: Typical voltage charactistics at various rates of discharge at 21 °C 1.5V rechargeable lead-acid battery

1.1 STATE OF CHARGE - SOC

To define the SOC has to be considered a completely discharge battery, with $I_b(t)$ charging current. The charge stored in the battery until the time τ is: $\int_t^{t_0} I_b(\tau)$; and the total charge hold by the battery is: $Q_0 = \int_\infty^{t_0} I_b(\tau)d\tau$

$$SOC(t) = \frac{\int_t^{t_0} I_b(\tau)}{Q_0} \times 100 \tag{1.3}$$

Usually, the SOC of the battery has to be kept between appropriate limits: $20\% \leqslant SOC(\%) \leqslant 95\%$ A possible way to estimate the SOC is by direct application of (1.4), but this is subjected to biases as it is a pure integration. Another approach is computing the open circuit voltage of the battery (the voltage when the battery current is zero). It has been shown that there is a linear relationship between the state of charge of the battery and its open circuit voltage in [5].

$$V_{oc}(t) = a_1 \cdot SOC_{\%}(t) + a_0 \tag{1.4}$$

$$SOC_{\%}(t) = \frac{V_{oc}(t) - a_0}{a_1} \tag{1.5}$$

Where a_1 is the battery terminal voltage when SOC is 0, and a_1 is the V_{oc} at 100% SOC, and the SOC is expressed in percentage, so by the 1.4, the estimation of the SOC can as well done as the estimation of the its open circuit voltage. From the 1.5 it can be seen that the estimation of the SOC is equivalent to the estimation of V_{oc} if V_{oc} at SOC= 0%, and V_{oc} at SOC =100% are known.
Unfortunately V_{oc} is still unknown, because it isn't possible to disconnect the battery (see 1.0.2).

1.1.1 *State of Charge: Determination-Methods*

There are many variables to consider in order to decide the state of charge of the batteries. These variables have also a causal relationship, making it difficult to estimate the state of charge accurately. There are some common methods to estimate the state of charge [11]. These are the following:

- Open circuit Voltage SOC
- Load Voltage SOC
- Coulomb SOC
- Load Voltage SOC
- Internal resistance SOC

Open circuit Voltage SOC

The open circuit voltage measures the voltage between the poles of the battery as it is in figure 9, the open circuit voltage of a lead-acid battery and charge storing inside of the battery are close to linear proportion: the higher the open circuit voltage of the batteries is,the higher the charge will be inside. Furthermore, the user have to measure with the open load, and put the battery for a while, so that the thickness of the electrolyte distributes well-mixed, and this is not possible. So the user has to combine other methods to determine the SOC.

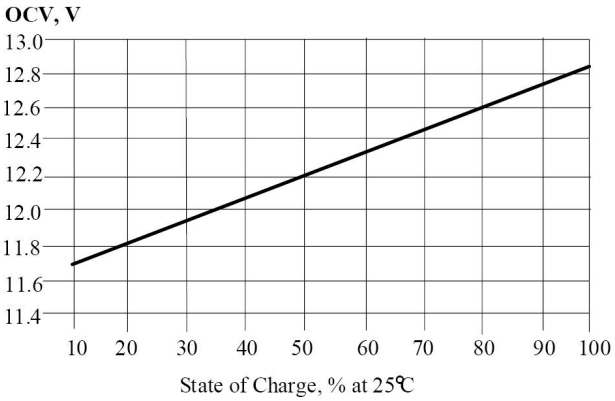

Figure 9: Open circuit voltage versus SOC [11]

Open Circuit Voltage vs. State of Charge Comparison*

% Charge	Open Circuit Voltage Flooded	Gel	Absorbed
100	12.70-12.60	12.95-12.85	12.90-12.80
75	12.40	12.65	12.60
50	12.20	12.35	12.30
25	12.00	12.00	12.00
0	11.80	11.80	11.80

NOTE: Divide values in half for 6-volt batteries.

** The "true" O.C.V. of a battery can only be determined after the battery has been removed from the load (charge or discharge) for 24 hours.*

Figure 10: Open circuit voltage versus State Of Charge (reported as in [14] pag.13)

Load voltage SOC estimation

The next Figure 11 shows the relationship between load voltage and state of charge when a lead-acid battery discharges with constant current. Loading voltage SOC estimation has the advantage to be simple and cheap (if the linear curve before the knee is used to predict the SoC, and the knee voltage to announce the discharge), but changing the load of the unfixed, discharge current it will cause faulty values. This method is useful if the user can´t stop for a while the battery to measure the voltage, so the user can only use load voltage. The discharge reaction reduces H_2SO_4 and increases H_2O, so the density of the electrolyte decreases as the SOC decreases. The next equation (1.6) shows the electromotive force (E), decrease as SOC increases.

$$E = 2.04 + 0.0591 \lg \frac{a_{H_2SO_4}}{a_{H_2O}} \tag{1.6}$$

Equation 1.6 points out, that when the battery is discharged the terminal voltage drops, because of the inner resistance. Before the sudden voltage drops the SOC is estimated as it is shown in equation 1.7

$$SOC = \frac{V - 11.7}{12.8 - 11.7} \times 100 \tag{1.7}$$

when V is the battery voltage.

$$C = \alpha V + \beta \tag{1.8}$$

Where α and β are parameters decided by the data (extrapolated by the fitting the straight line to the curve that represents the load voltage versus SOC). The difficulty of this estimation method is that the measured voltage suddenly drops under end-of-charge voltage (knee voltage) at the end of the discharge process. Besides the parameters α and β change with the current required from the battery, because the terminal voltage is different at a different current. Unfortunately, in

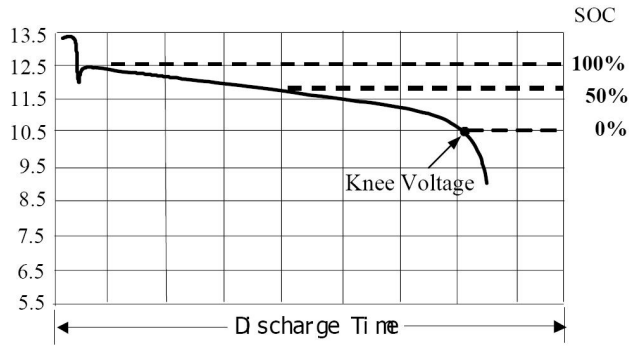

Figure 11: Load voltage versus SOC [11]

case of the pulse discharging, the estimation of the terminal voltage is very difficult by reason of non-uniform distribution of the electrolyte around the electrolyte causes the terminal voltage to vary in a short time.

Coulomb SOC-Current integration

This method uses ampere-hour and it is based on calculating the residual charge stored in the battery. It takes into account the charge that the battery provides to the load as follows: NEW SOC = OLD SOC +/- amount of charge / discharge. If the total integration of the charged current is correctly known, the SOC is estimated by integrating the discharge current. It is difficult to integrate the discharged current. And even if the amount of the charge is known, the state of the previous discharge has an effect on the SOC. This points out the drawbacks of this method.

INTERNAL RESISTANCE AS FUNCTION OF SOC

Internal resistance SOC

The internal resistance [8] is a gross value comprehensive of a number of small contributions like resistivity of the plate grids, the lead posts and the interface contact resistance between these parts, and the most importantpoint is, that contribution comes from the electrochemical system of the cell, including resistance to ionic conduction within the electrolyte, the interface the electrolyte with the active materials of the plates, and the resistivity of the active materials with the plate grids ([1][Par4.1.4.1-Pag.167]). The chemical contribution to the resistance of the battery is produced with polarizing in an electric chemical reaction [11]. In effect when the cell is fully charged, the electrolyte is at its highest state of concentration (highest specific gravity). As the cell discharges, the sulfate ion concentration decreases, like the thickness of the electrolyte, and so the internal resistance will increase[11], because related with the ion concentration. In effect this reduction in available current carriers is seen as higher internal resistance in the Thèvenin equivalent circuit [1]. The figure 12 shows this relationship. Notice that substantial impact occours until the cell state of charge falls below 25%. When the cell state of charge falls below 25% towards zero, the resistance has got a dramatic improvement [1].

The value of the internal resistance will change with the thikness of the electrolyte which is decided by the charge inside the battery, so the internal resistance will decrease when the battery charges, and increase when discharging, beacuse the thikness of the electrolyte of the battery decreases.

Because the changing of the internal resistance inside the battery is very little, the equipment measuring the internal resistance needs high accuracy and precision. Besides, the internal resistance of the battery will have non-linear changing, because of the aging of the battery, which not only affects the accuracy of the detecting, but also makes it hard for the user to correct and adjust.So it is very difficult to reckon the accurate state of charge by using the internal resistance [11] pg 2019. With a fitting function is also possible to find out the relationschip between Internal resistance and SOC like showed in Figure 12, and comparing it with Peuchert's Equation.

Model of internal resistance

A model of the internal resistance used during a pulse discharge,

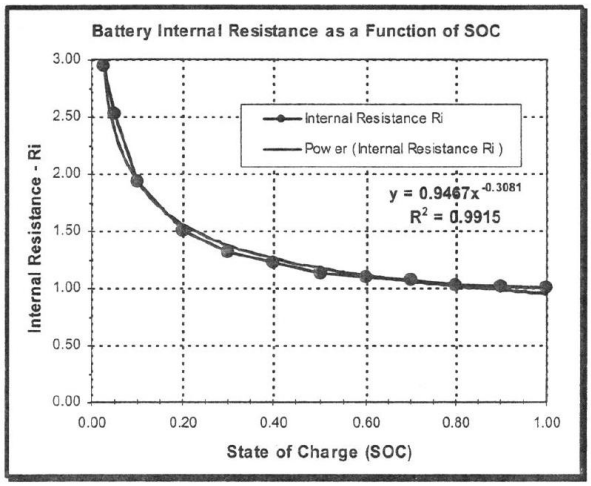

Figure 12: Internal resistance versus SOC [8]

and voltage and current waveform are showed in fig 13. R1 is the electrolyte resistance including the electrode resistance. R2 is the charge transfer resistance at the interface between the electrode and electrolyte solution, and C is the electric double layer static capacity formed at the interface between the electrode and electrolyte solution.

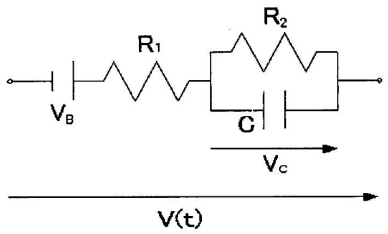

Figure 13: Inner resistance battery model usinf pulse discharge [7]

The equation that describes the terminal voltage

$$V(t) = V_B - I(R_1 + R_2) + R_2 I e^{-\frac{t}{CR_1}} + V_c e^{-\frac{t}{CR_2}} \tag{1.9}$$

in steady state the equation becomes:

$$V(t) = V_B - I(R_1 + R_2) \tag{1.10}$$

and from this is obtained the following expression for the inner resistance:

$$R_1 + R_2 = \frac{\Delta I}{\Delta V} \tag{1.11}$$

where ΔI and ΔV are the amplitudes of the pulse signal $\Delta I = I_{pp}$; $\Delta V = V_{pp}$ In figure 14 an example of the inner resistance calculated as shown before is depicted.It is possible to estimate the SOC from the inner resistance to a certain degree. The value of the inner resistance can be expressed as a parabola as a function of the SOC:

$$SOC(t) = \frac{\alpha}{R - \beta} + \gamma \tag{1.12}$$

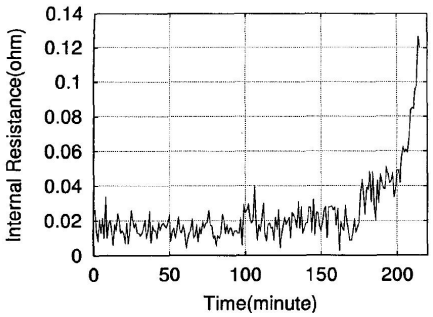

Figure 14: Inner resistance versus time[7]

the tree parameters α, β, γ are decided by fitting the parabola to the graph with a non linear least square in figure 14. The problem relating the determination of this parameters are: that they depends on the temperature, the value of the internal resistance has got large noise (1.12). In [7] it is proposed how to estimate the SOC. The equation to estimate is (1.13)

$$SOC^* = \alpha V + \beta R + \gamma\sqrt{V} + \delta\sqrt{R} + const \tag{1.13}$$

The characteristic of this equation is, that the square root about the terminal voltage and internal resistance employed for estimation. So, it should be noticed, that:

- SOC^* = estimated SOC
- V = terminal voltage
- R = Internal resistance

In [7] it is shown, that the parameters in equation 1.13 are estimated from the measured data by the least square error (LSE) method. The results of this estimation method are:

α	243.11
β	- 8.01
γ	-1599.73
δ	4.32
const	2631.37

Table 1: Estimated Parameters

This estimation method has got a little estimation error also when the SOC graph bends and it becomes difficult to estimate. [7]

1.2 BATTERY MODELIZATION

It is already known, that the internal resistance differs under discharge and charge conditions, so a complex model is needed to describe the internal dynamics of the battery: in particular the effect of the diffusion of the electrolytic chemicals between the battery plates.

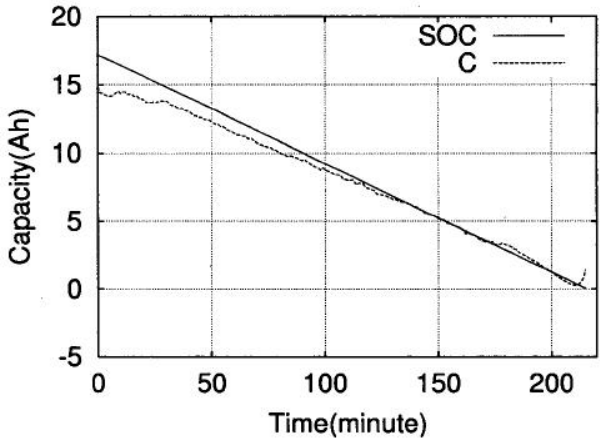

Figure 15: SOC estimated and real [7]

To take in count the different resistance values under charge and discharge conditions, the circuit can be modified as shown in figure 16 (in [12]figure 2).

Different resistance values on Charge/discharge conditions

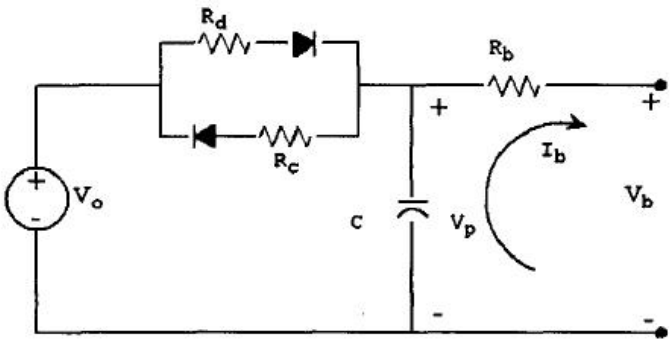

Figure 16: Battery modelization accounting for the different values of resistance in charging and dischargin battery and capacitor to take in count polarization effect.[12]

The diodes has no physical meaning: they only need to enable one of the resistors and disable the other, in order to model the diffusion of the electrolytic through the battery and its resultant effect of causing transient currents in the battery, a capacitor is added to the model as shown in figure 16. [from [5] and [6]]

This is the model adopted here to develop a state of charge estimation scheme. The equations that describes the circuit are :

$$\dot{V_p} = -V_p \frac{1}{R_d C} + V_{oc} \frac{1}{R_d C} - I_b \frac{1}{C}, (V_P \leqslant V_{oc}) \tag{1.14}$$

$$\dot{V_p} = -V_p \frac{1}{R_c C} + V_{oc} \frac{1}{R_c C} - I_b \frac{1}{C}, (V_P > V_{oc}) \tag{1.15}$$

$$I_p = \frac{V_p - V_{oc}}{R_b} \tag{1.16}$$

The current I_b is considered to have a *positive sign* during discharge(the capacitor modelize the *polarization capacitance* and model the chemical diffusion within the battery (its value depends on SOC, temperature and also the device design). None of the parameters R_c, R_d, C are known a priori and V_p is not measurable. The problem then is to estimate V_{oc}, (the SOC is then found using 1.5) with only measurements of the terminal voltage and current [12] .

2 CHARGE EQUALIZER SYSTEMS

Imbalance of cells in battery systems is very usual, like differences in internal impedences and in self-discharging rates (different characteristics) indeed, they differ in their behaviour. To maximize the capacity and reliability, the individual battery voltages in a battery series must be totally uniform [16]. Once the imbalance occours, it will increase with additional use. For lead-acid batteries the gassing phase is not a big problem, despite the fact, that it causes overheating and loss of electrolyte. Also excessive low voltages during the discharging process imply a low acidic concentration of the electrolyte. During the next charge period, some of the lead precipitates into partices called dendrites. These dendrites create current leakage paths between the electrodes, and may result in a short circuit. Therefore the battery can be damaged by excessive high or low voltages [21].

2.1 GENERAL REVIEW ABOUT CHARGE BALANCER

Balancing is the most important concerning relating the life of the battery system, because without the individual cell voltage, it will drift apart with time figure 18. The theory concerning the proposed balancing methods will be presented here.Balancing methods can be passive or active. Passive

active balancing

Active balancing instead, uses external circuits to actively transport energy among cells in order to balance them. This method is the only applicable with Lithium based batteries; because it avoids the gassing phase allowing a constant battery temperature. Active balancing methods can be sorted by circuit topology: *Shunting methods*, *Shuttling methods*, *Derivative methods*.

Short overview of all methods

It is hard to find one method for all applications, because the methods range has limited effectiveness; otherwise it will be exorbitantly expensive. The balancing methods are grouped in 3 categories according to their nature of balancing. Dissipative resistor, Boost shunting, and Switched capacitors are three methods for different applications.

Dissipative Resistor (in CCM) is good for low power applications. Indeed for low power applications the resistors can be small and don't need much thermal management, and it is really cheap.

Boost shunting is good for either low power applications. The relatively low costs and the relatively simple control makes it a good candidate for many applications.

Switched capacitor is good for HEV (Hybrid Electric Vehicles) applications; not only because it is able to operate during the charging and discharging phase, but also because it has a very simple control.

2.1.1 *Shunting active balancing method*

how is works

This method removes the excess energy from higher voltace cells to let them wait for the lower voltage cells to catch up with them. There are two kinds of shunting methods:one using dissipative methods, and the other non-dissipative methods, regarding the application, a good balance between heat dissipation and effectiveness of balancing must be made, since excessive heat dissipation will increase the difficulty of thermal management.

Dissipative shunting resistor method

The dissipative shunting resistor method is a very reliable and simple one. The basic circuit topology is shown in fig.:17. The same topology can work in two modes: continuous and detecting mode. In the *continuous mode* all switches are controlled by the same signal at the same time; they will be turned on only during charging: the cells with a higher voltage will have less charging current, so as to wait for the other cell to be charged. Care must be taken to choose properly the resistor. The advantage of this mode is, that it doesn't need a complex control for it. In contrast, the *detecting mode* , needs to monitor the voltage of each cell: an intelligent controller senses the imbalance conditions and determines if the dissipative resistor must be connected to remove the excess of energy from the cell. In both methods the value of the resistor should be determinated according to the application. For example, if the dissipating current is smaller than 10mA/Ah (a 10mA/Ah could balance cells at a rate of 1% per hour), so this circuit could drain the battery pack in few days (more than 4 days). This topology is not a very effective active balancing method. It could be used in many applications for low-cost solutions [15]. Another method could be dissipative shunting: it shares the same idea, but instead of using resistors, it uses transistors as the dissipation component.

Continuous mode

Detecting mode

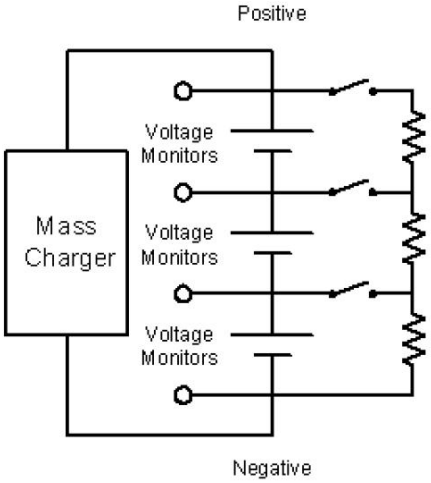

Figure 17: Basic disspiative resistor topology [15]

could be used for a low-cost solutions

PWM controlled shunting

This is a kind of a non-dissipative method where the Battery Management System (BMS) senses the voltage difference of the two neighboring cells: by applying a PWM square wave on the gate of the pair of MOSFETs, the BMS controls the current difference of these two cells. In this way the average current flowing through the higher voltage cell will be lower than the normal cell. Disadvantages of this circuit are that it is complex, it needs accurate voltage sensing and $2(n-1)$ switches and n-1 switches for n cells [15].

how it works

advantages and drawbacks

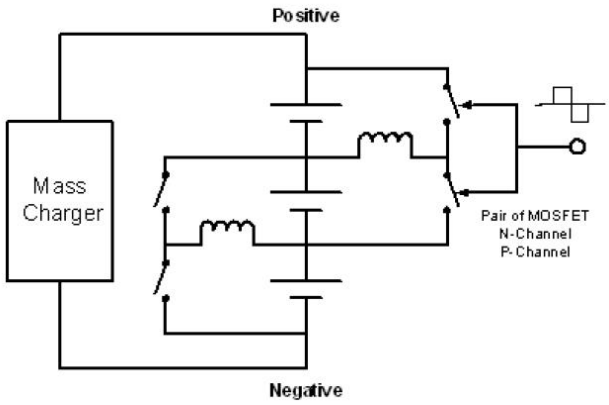

Figure 18: PWM controlled shunting [15]

Resonant Converter

It is another version of the previous, but instead of using intelligent control to sense and generate PWM gating signals, it uses a resonant circuit to both transfer energy and drive MOSFETs [15]. Figure 19 shows the resonant converter balancing circuit: L1 and C1 is used to both transfer energy and drive the MOSFET. When the voltage across L1 is positive, Q2 is on; otherwise Q2 is turned off. The resonance will cause a reverse current through L1, turning off Q2 and turning on Q1: in this way a new cycle of resonance is started. If cell 1 has got a higher voltage than cell 2, the average current flowing through inductor L2 will be positive to balance the two cells. This topology is complex, and needs a resonant startup circuit [15].

how it works

advantage and drawsbacks

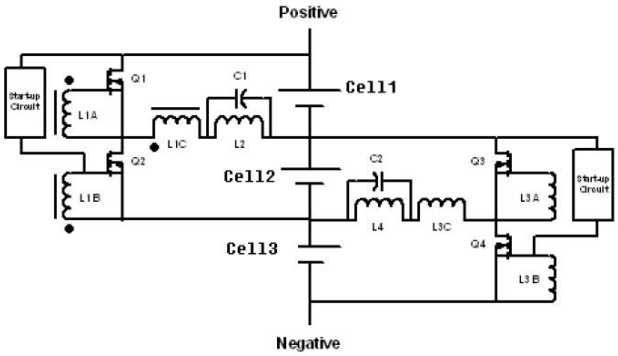

Figure 19: Resonant Converter balancing [15]

Boost Shunting

how it works

In the boost shunting method, individual cell voltages are measured and switched for to the cell with higher voltage will be activated by the main controller. The switch is controlled by the PWM signal. Figure 20 shows the boost shunting circuit. When it is working, the circuit is actually acting as a boost converter. The boost converter diverts the extra energy to the other cells in the string. The equivalent circuit is shown in figure 20. This circuit is relatively simple and fewer components are used as compared to other advanced balancing methods.

advantages and drawbacks

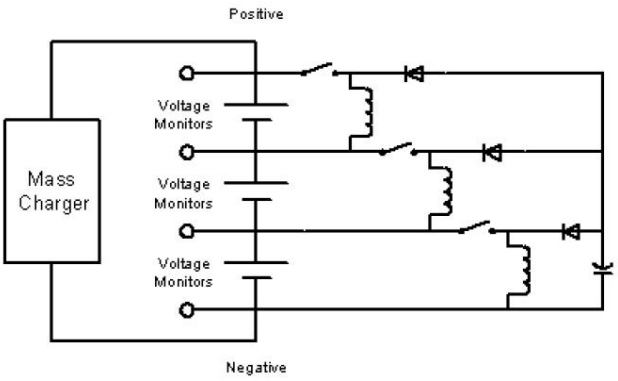

Figure 20: Boost Shunting [15]

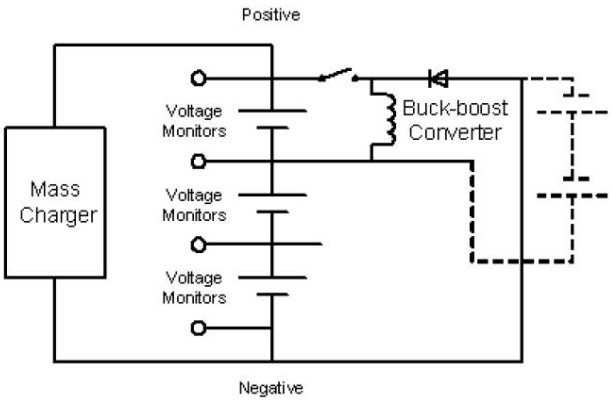

Figure 21: Boost shunting equivalent circuit [15]

Complete Shunting

how it works

Complete Shunting is shown in fig.: 22: in this circuit a mass charger (a current controlled converter) is needed. When one cell reaches its maximum voltage, the cell is completely shunted by using two switches. The charge finishes until the last cell in the string is fully charged. When a string is long, it may need a cascade buck converter for which the output voltage range is very wide. This topology is used in expensive UPS: for best results cells must be individually charged. It also requires an expensive parallel charger [15].

advantages and drawbacks

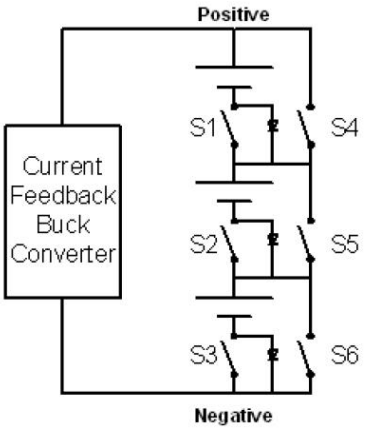

Figure 22: Complete shunting [15]

2.1.2 *Shuttling active balancing methods*

This kind of method uses external storage devices (typically capacitors) to shuttle the energy among the cells to balance them. There are two shuttling topologies: the *Switched capacitor* and the *Single switched capacitor* [15]

Switched capacitor

how this topology works

This topology requires, 2n switches and n-1 capacitors in order to balance n cells. The control strategy is very simple, because there are only two states. Capacitor C1 will be paralleled with B1 and C1 will be charged or discharged to obtain the same voltage as B1. After this process the system will turn to the other state: C1 paralleled with B2. The same thing as in the previous state will happen. After cycles of this process, B1 and B2 will be balanced and so on. So, the total battery pack can be balanced. The advantages of this topology are, that it doesn't need an intelligent control and it can work in both recharging and discharging operation. This topology reqires $(n-1)$ capacitors to balance n cells [15].

advantages and drawbacks

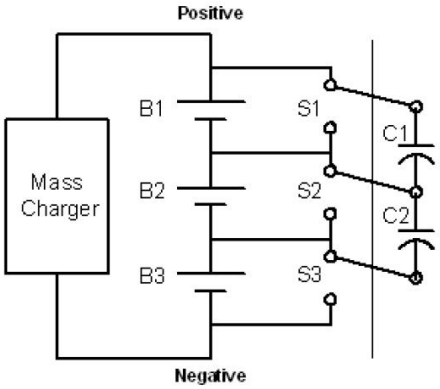

Figure 23: Switched capacitor topology [15]

Single Switched Capacitor

This method uses only one capacitor to shuttle the energy. If a simple control strategy is used, and n is the number of cells, the speed of balancing is only 1/n of the regular switched capacitor method. For this topology also n switches are needed. A more advanced control strategy can be used to switch between the highest and the lowest voltage cell (cell to cell method) . With this method the balancing speed will be much higher, too (fig.:24). For this topology n switches and one capacitor are needed to balance n cells. It needs external devices to store energy shuttled [15].

necessity of a more advanced control

little overview of drawbacks and advantages

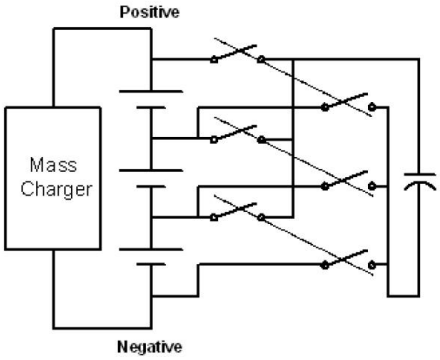

Figure 24: Single switched capacitor topology [15]

2.1.3 *Isolated converter active balancing method*

In these converters the input and output have isolated grounds [15].

Step-up converter

This method uses insulated boost converters to remove the excess of energy from the single cell to the total pack. The inputs of the converters are connected to each cell to be balanced fig.:25. The outputs of the boost are connected together to the total battery pack. The control senses the voltage of the cells and commands the operations to balance the cells. This method is relative expensive, but suitable for modular design. Special consideration is needed if the battery pack has very long string cells, because the step-up converter needs to boost a single cell voltage to the pack voltage [15].

advantages and drawbacks

Multi-winding Transformer

In the Multi-winding Transformer topology, a shared transformer has a single magnetic core with secondary taps for each cell. Current from the cell stack is switched into transformer's primary winding and induces current in each of the secondary windings. The secondary winding with the least reactance will have the most induced current. The transformer must be customized according to the number of cells. The disadvantages of this topology are the complexity and the high costs [15].

advantages and drawbacks

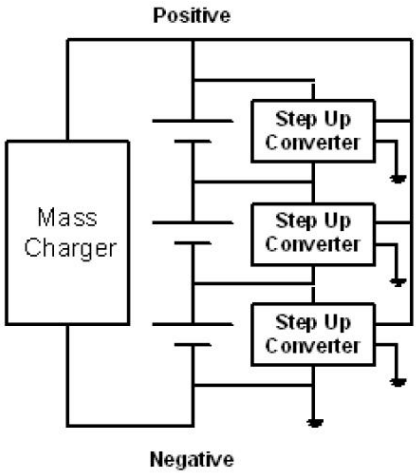

Figure 25: Step-up converter topology [15]

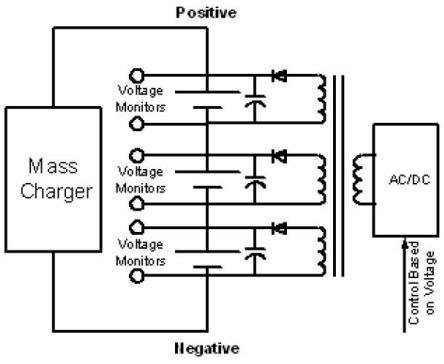

Figure 26: Multi winding transformer topology [15]

Ramp Converter

how it works

It shares the same idea as Multi-winding Transformers. It requires only one secondary winding for each pair of cells instead of one per cell. While operating, on one half cycle, most of the current is used to charge the odd number of lowest voltage cells while on the other half cycle, most of the current is used to charge the even number lowest voltage cells via the so called ramp [15].

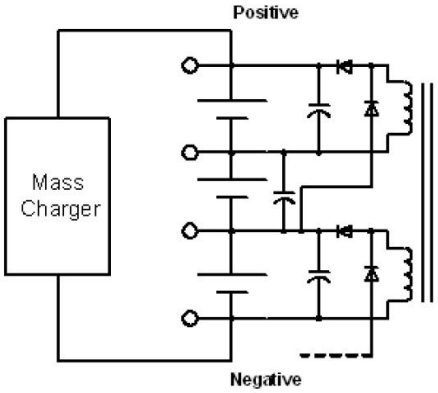

Figure 27: Ramp converter topology [15]

Multiple Transformers

In comparison with the multi-winding transformer scheme, this topology is better for modular design [15].

Switched Transformer

how it works

It is a selectable energy converter: the input is connected to a series of switches, which are used to select which cell the output connects to. The controller detects the unbalanced cell and then controls the switches to connect the isolated converter to it [15].

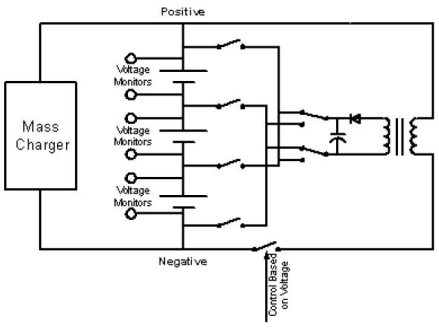

Figure 28: Switched transformer topology [15]

2.1.4 *Charge Equalizer for long strings of battery*

For large numbers of cells (eighty or more), a charge equalizer method could be based on a battery modularization technique. In this method

a very long battery string is divided into several modules, and then an intramodule equalizer and outer-module equalizer are designed. Thus, the design of a charge equalizer becomes easier.Battery strings connected in a series have been used in several applications such as: uninterruptible power supply (UPS), electrical vehicles (EV) and hybrid electrical vehicles(HEV). Especially in HEV, the repeated charge and discharge phenomenon (due to regenerative breaking), causes a cell mismatch problem, because batteries have inevitable differences in chemical and electrical characteristics from manufacturing. If these imbalanced batteries are left in use without any control, the energy storage capacity decreases severely, and in the worst case there may be an explosion or fire. The conventional charge equalizer systems can be classified in two categories:the *dissipative* (2.1.1) and *non-dissipative method*, as showed in the chapter before. The non-dissipiative type can be divided into three parts: charge type, discharge type and a composite charge-discharge type [16].For a small amount of cells, automatic or selective equalization based on multi-winding transformer have been achieved, but for big amount of cells, for example more than 80 cells stacked in series to obtain a DC source of more than 300V, the previous approach tends to produce some problems. Such problems include difficulties on implementing a multi-winding transformer, the prolonged equalization time (cell-to-cell shift) and the complexity of controlling a large number of DC-DC converters. To avoid these problems, a charge equalizer method based on battery modularization technique is presented in this article [16]. A long battery string is divided into several modules and then an intra-module equalizer and an outer-module equalizer are designed. This technique reduces the number of cells that is needed to take in count when the design of charge equalizer must be done. If more batteries are stacked in

safety problems if charge is not equalized

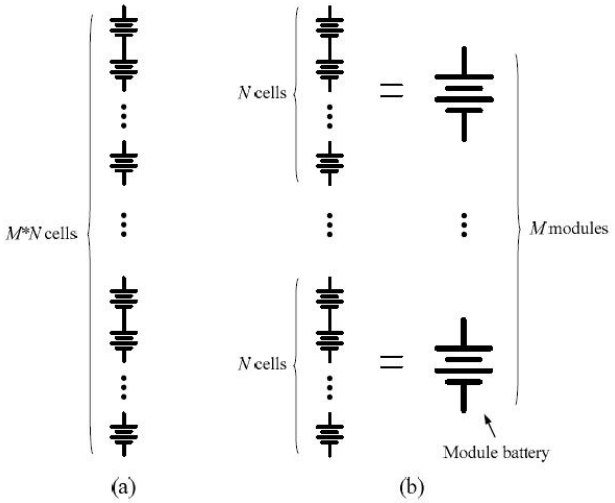

Figure 29: Battery string configuration (a) Conventional structure; (b) Modularized structure [16]

a series to obtain a DC source of a big voltage, for example in automotive applications more than 300V could be required and could need approximately more than 80 batteries in stack. In those cases

Charge Equalizer applied to mode than 80 batteries

there are difficulties to implement a Multi-winding Transformer . The problems that arise with a great amount of cells are

- Implementation possibility
- Equalization speed
- Equalization efficency
- Controller simplicity
- Circuit size and cost
- Mismatched leakage inductance

To avoid these problems in [16] is a charge equalizer design method proposed, based on a battery modularization technique. A long string of battery is divided into M modules, where each module is composed by N cells as shown in Figure 29; then an intra-module equalizer and a outer-module equalizer are designed. This modularization technique effectively reduces the number of cells which must be taken into account designing a charge equalizer. In [16] an example is shown with two modules, each one composed by four cells. The multi-winding transformer based balancing scheme is applied to both intra-module equalizer and the outer-module equalizer;in [16] are also compared the classical and modularized approach of two topologies: *multi-winding transformer* and *switched capacitor*. The *switched capacitor* with modularized approach in [16] is implemented with *cell-level switched capacitor system* for intra-module, and *module-level switched capacitor system* for the outer-module as in fig.:30. *Cell-*

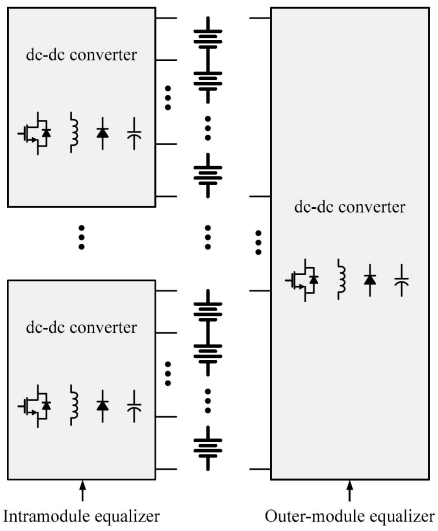

Figure 30: intramodule and outer-module charge equalizer structure [16]

level and module-level Switched Capacitor System are shown in fig.:31 two MOSFET (n-Mos and p-Mos) switches are connected to the battery: one to the positive and the other to the negative terminal. The drain terminal of both switches are connected , and this point is coupled with the equalizing capacitor C_7. The complementary gate signals S_{HD} and S_{LD} are fed to two insulated gate drivers OC_3 and

OC_4. The only difference between *Cell-level* switched capacitor and *Module-level* Switched Capacitors, is that the last one has a improved performance on driving the gate and that the voltage rating of the MOSFET switches is upgraded due to the higher voltage of the module battery. The experiment presented in [16] is conducted with a 7Ah HEV lithium-ion batteries of which the maximum discharge current is about 200A. Under these conditions:

- The same cell voltage distributes at the beginning of equalization
- The same PWM modulation control was applied
- Approxmimately 3.5 hours of equalization time, and one hour of idle time
- all of the cell voltages were monitored every 10 seconds

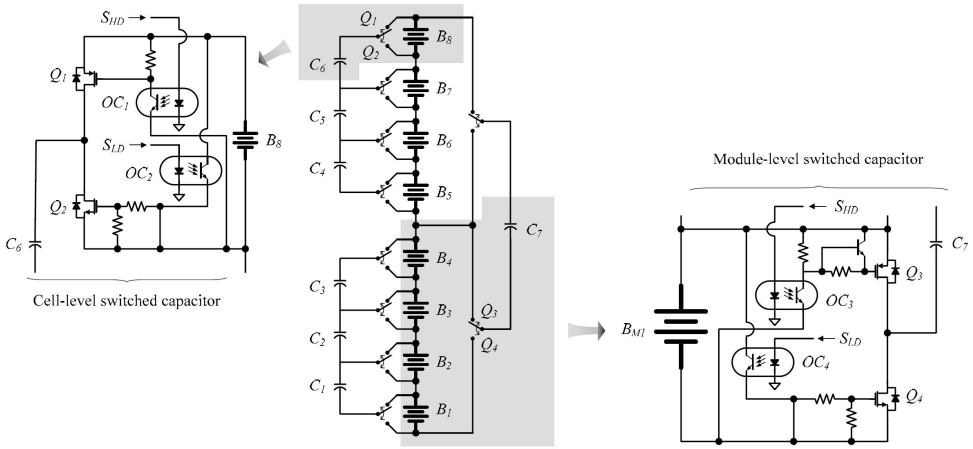

Figure 31: Switched capacitor-based modularized charge equalizer [4]

The comparative results are presented in figure 32; so it is possible that at the end of balancing the maximum voltage gap among the cells is reduced with the modularized approach, if compared with the conventional equalizer. If this modularized charge equalized scheme is applied to a very long string of batteries the benefits outweigh the drawbacks of increased size and costs [16].

2.1.5 *Little focus on the Switched Capacitor topology*

In the switched capacity topology, the equalization of the cell voltages can be obtained by alternatively switching a suitable capacitor or an accumulator parallel to the cells as shown in fig.:33. If the voltage of the selected cell is higher than the capacitor voltage, a corresponding amount of charge is transferred to this cell. If the switching frequency is chosen high enough (some 100Hz), this charge transfer produces an equalization of cell voltages. This system works during charging as well as during discharging of the battery. It can be stepped up in a modular way and can easily be adapted to existing battery systems

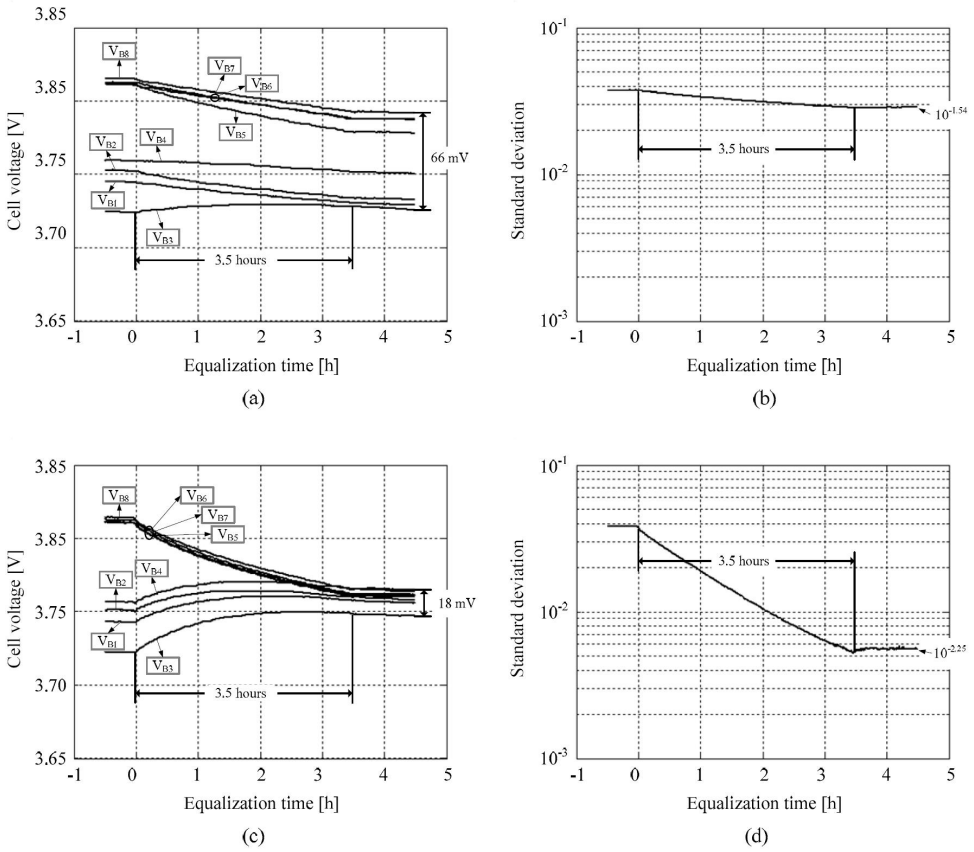

Figure 32: Equalization performance comparison: a, b conventional approach; c,d modularized approach [4]

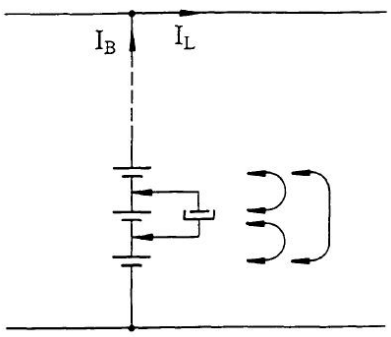

Figure 33: Charge transfer by a switch capacitor [19]

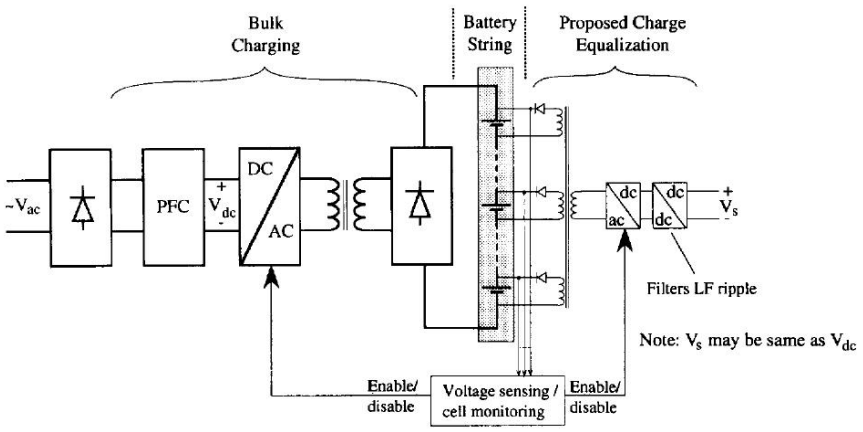

Figure 34: Block diagram of a charging system showing bulk charging and the proposed charge equalization scheme [24]

[19]. The [20] switched capacitor approach performs equalization on the same time scales as active methods if the switching frequency is selected properly. *The capacitor value is not relevant to the final result*, but only to the rate of the charge exchange. The switching process must be fast and the switches must exhibit no voltage drop as the current decrease to zero. Each switch needs to block only the voltage of a single battery (rarely more than 15V). The capacitors requires also 15V ratings. Appropriate values will be in the range of 20µ F to 1000µF.

2.2 CHARGE EQUALIZER FOR SERIES CONNECTED BATTERY STRINGS-DC /DC CONVERTER TOPOLOGY

bulking phase

During the bulking charging phase, each cell (or stack of cells) are monitored; if any of these cells reaches its nominal voltage or if gassing is detected, bulk charging is shutted off and charge equalization is enabled. The basic technique utilizes a simple insulated dc/dc converter with a capacitive output filter analog with a multi winding coaxial transformer (known for low and controlled leakage inductance and accurate control of all fluxes). In fig.: 34 a block diagram of the proposed charge equalization scheme is shown. The transformer leakage inductance is used as the main driving impedence to control the total charging current. Assuming only one winding for the transformer secondary, as shown in fig.: 35, it can be seen that the transformer, and thus the battery charging current is governed by the forward converter voltage V_s, the battery stack voltage V_b and the leakage inductance L_s

basic techinque for charge equalizer

usage of the leakage inductance

$$I_{ch}(t) = \frac{aV_{in} - V_b}{L_S} \tag{2.1}$$

Figure 35 shows an extension of the single cell to cells. It is seen that with low-leakage inductance and controlled V_S, the lower voltage cell can be designed to draw significantly higher current as compared to the other cells. This will then charge the lower voltage cell until the

voltages become equal at which point charging can be tapered off via V_S control using a buck converter or similar arrangement. By controlling V_S, one can have even greater flexibility in directing charge to those battery cells in need of more charging. It provides also a means of tracking the nominal battery voltage as it varies due to temperature and aging effects. In principles the scheme can be extended to multiple cells all operating from one single converter, as shown in fig.: 34. To implement this topology a coaxial winding transformer which is simple in structure, easy to manifacture and tightly controlled parasitics is needed. The transformer needs to be optimized, so that the full converter rating can be used to charge the weakest cell. Once the final equalization voltage is reached, the converter can be turned off.

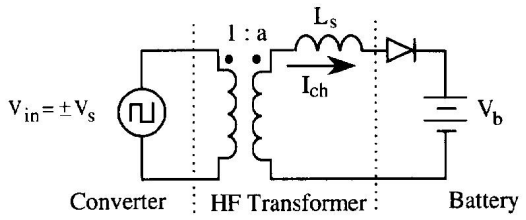

Figure 35: Basic converter winding transformer [21]

2.3 REVIEW ON EQUALIZATION METHODS

necessity of a charge equalizer

To maximize capacity and reliability, the individulal battery voltages in a series connected pack must be uniform. Indeed during a charging and discharging cycle, batteries may not operate in a uniform manner. For lead-acid batteries the charging period can be splitted up in two periods: the bulk charge period and the trickle charging period. The last one represents the equalization of the charge. Most of the charge is provided in the bulk phase, (current can reach the 240A); when the voltage can reach a certain level, a trickle charge is applied for several hours at low current (about 1A dc) and each battery will reach its full charge and any excess of charge will be dissipated safely in the battery . Trickle charging is unacceptable for high performance batteries like lithium-ion, because those can explode if overcharged. For this reason a more clever Charge Equalizer system is needed. In selective Buck-Boost Charge Equalizer it is looked for routes all of the equalizing current only to the weakest batteries [21].

bulk-trickle charge

Switched Capacitors

- *Switched Capacitors* or DC/DC converter. A pulse transformer is used to drive the switches. The switches experience high surge currents, especially when large voltage imbalances are present. The impact of the electromagnetic interferences could be also relevant, but the most important thing is the energy dissipation that is proportional to the square of the voltage stored by the capacitor.

Buck-boost

- *Buck Boost Isolated Equalizer* Usually a separate transformer secondary winding and rectifier are used for each battery. The converter is operated as a constant current source, and each battery

is effecttively parallel connected with the converter output. (the battery with the lowest voltage will draw a significantly higher current than the other batteries. The circuit achieves the buck-Boost operation when the input to the converter is connected across the total battery pack). This should provide good equalization, but the traditional design is complex and may have a relatively high number of elements. Establishing a battery stack parallel to the capacitor stack could be also useful, in the aim on having an energy and power tanks. The power tank can be represented by a super capacitor

Ramp converter

- *Ramp Converter* This topology inherits its name from the shape its primary current waveform. The input is normally connected across the entire batteries pack, and the energy is transferred from the higher to the lower voltage batteries. The total equalization current is regulated by means of frequency modulation, and the circuit is arranged so that all power semiconductors employ ZVS (Zero Voltage Switching) and/or ZCS (Zero Current Switching). This could provide very low losses in the switches, so frequency can get higher and the size and cost of the circuit can be minimized. Unfortunately, the differences in the transformer secondary leakage inductances can affect the equalization currents.

drawback

- *Selective Ramp Equalizer* (should improve the performance of the earlier Ramp Equalizer) It uses bipolar transistor switches to handle the equalization current. These scheme eliminates the necessity for balanced leakage inductances, and it also reduces the required power level.
  In [21] it is evidenced, that a normal use is not a very practical means for comparing equalizers. If a very good pack is used it is very difficult to determine relative performance between CE, because all equalizers will product good results. Also in some packages some types of batteries might require 25 or 30 charge/discharge cycles of several hours each to produce a significant imbalance, and a similar number of cycle of charge and discharge to correct it; beside the battery characteristics change as the pack is cycled.

basics on how to make a comparison between CE

3

MUTUAL INDUCTOR DESIGN

The aim of the circuit is to transfer some of the power from a battery to another without a binding discharge. Supposing to have a 12Ah battery with a fully charged voltage of 12V and a C1 discharge rate, it is possible to drawn a current of 1A. The power amount that has to be transferred through the mutual inductor is $12W = 1A \times 12V$. For this reason an average input current of $I_{dc} = 1A$ in the charge equalizer is required; a ripple of about 15% is imposed, that means $15\%I_{dc} \Rightarrow \Delta i = 150mA$.

$I_{dc} = 1A$

$$\Delta I = 15\%I = 150mA \tag{3.1}$$

L=400µH

With the applied battery voltage of $V_{IN} = 12V$, and assuming a duty cycle as $\delta = 1/2$ ($\Delta t = 50\ \mu s$), it is possible to calculate the value of inductance from Faraday's law:

$$V_{IN} = L_P \cdot \frac{\Delta i}{\Delta t} \Rightarrow L = 400\mu H \tag{3.2}$$

$$\begin{aligned} I_{rms} &= I_L \cdot \sqrt{1-\delta} \cdot \sqrt{1 + \frac{1}{3}\left(\frac{\Delta i}{I_{dc}}\right)} \\ &= I_L \cdot \sqrt{1-\frac{1}{2}} \cdot \sqrt{1 + \frac{1}{3}\left(\frac{0.1A}{1A}\right)} \\ &= 0.719A \end{aligned} \tag{3.3}$$

$I_{rms} = 0.719A$

The efficiency required for this charge equalizer is: $\eta \approx 98\%$; indeed it must be as high as possible, otherwise this device will not work properly.

$$P_{diss} = P_{trans} - P_{trans} \cdot 98\% = 240mW \tag{3.4}$$

$\eta = 98\%$

$$P_{diss}^{core} = P_{diss}^{winding} = P_{diss}^{tot}/2 = 120mW \tag{3.5}$$

3.1 CORE DESIGN

3.1.1 *Ferrite selection*

The core temperature is supposed to be of about 80°C; and an environmental temperature of 40°C, resulting on a temperature improvement of $\Delta T = 40°C$. As suggested in figure 36 reported from Epcos data sheet, N87 ferrite material is the best choice for switching frequency of $f_{sw} = 100kHz$.

selection of the ferrite type

	ΔT_{max} K	f_{typ} kHz	f_{cutoff} kHz
N59	30	750	1500
N49	20	500	1000
N62	40	25	150
N27	30	25	100
N67	40	100	300
N87	50	100	500
N72	40	25	150
N41	30	25	100
N61	30	25	150

Figure 36: Core selection: usage of ferrite type suggested from Epcos and the associated typical an maximal work frequency ([29] pg139)

3.1.2 *Core selection*

In order to be able to store energy in the mutual inductor, an air gap is required. To estimate the inductance value calculated for an existing gapped core, (pag 5-7 [26]) with a given number of turns, as first approach an **inductace factor:** A_L is calculated as provided in the formula (3.6) provided in [31]. In figure **??**, the suggested air gap value related to the nearest inductance factor value of $A_L = 347nH$, is 0.16mm. Applying N=35 turns, and a inductance value L=400 µH, it is obtained

$$A_L = \frac{L}{N^2} = \frac{400 \cdot 10^3}{35^2} nH \approx 326,5 \frac{nH}{turns^2} \tag{3.6}$$

Core selected EE25/13/7

The nearest value available in data sheet is $A_L = 347nH$; and the core that best fits to this value is EE 25/13/7 , whose characteristics are reported in figure 39. Within this specific core, the below maximal flux density is obtained (see (3.13)):

$$B_{MAX} = \frac{L \cdot I_{pk}}{A_e \cdot N} = \frac{400\ 10^{-6} H \cdot 1,075}{52,5mm^2 \cdot 35} = 234mT \tag{3.7}$$

It is pointed out that $B_{MX} = 234mT < B_{SAT} = 380mT$. This assures a safe saturation margin of about 40%. Below, important basic relations are presented.
Ampère's law gives the total magneto-motive force along any closed path with a length of l[m] that link together all N conductors:

$$F = \oint H dl = N \cdot I \qquad [J\ A] \tag{3.8}$$

Supposing that H is constant in the entire path, it is possible to substitute $H \cdot l = N \cdot I$:

$$mmf = F = N \cdot I \approx H \cdot l_e \ ; \Rightarrow l_e = \frac{N \cdot I}{H} \tag{3.9}$$

From Faraday's Law:

$$\frac{d\Phi}{dt} = -\frac{u(t)}{N}; \qquad \Delta\Phi = \frac{1}{N} \int u(t) dt \tag{3.10}$$

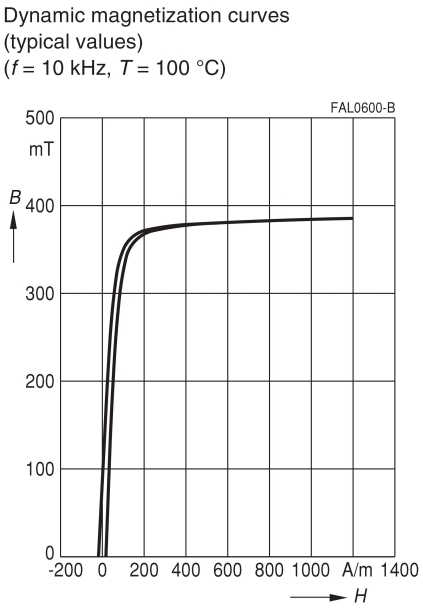

Figure 37: Flux saturation limits for N87 ferrite at 100°C and 10kHz. This picture shows that the upper bound is at 380mT - Epcos description core materials [28] pg82

When: u(t) represent the voltage across the winding; N represent the number of turns and Φ the total magnetic flux passing through a surface S having area A_e; it is so calculated:

$$\Phi = \int_S B \cdot d\overline{S} = B \times A_e \tag{3.11}$$

The last equation is valid for a uniform flux density of magnitude B through a constant area A_e. It is possible calculate the slope of the characteristic voltage-integral vs. current ($\int u(t)dt$ *vs* I) through the winding, that represents the inductance

$$L = \frac{\int u(t)dt}{I} = \frac{N^2}{\mathfrak{R}} = \left(\mu \frac{A_e}{l_e}\right) \cdot N^2 \tag{3.12}$$

When $\mathfrak{R}$ is the reluctance defined as $\mathfrak{R} = \oint \frac{dl}{\mu_0 \mu_r A_e}$.
Reminding relation (3.9) it is obtained:

$$A_e = \frac{L \cdot I}{\mu \cdot H} = \frac{L \cdot I}{B \cdot N} \Rightarrow A_e = \frac{L \cdot I_L^{pk}}{N \cdot B_{MX}} \tag{3.13}$$

$$A_w = \frac{A_{cu}^{TOT}}{K_w} = \frac{N \cdot I_L^{rms}}{J} \cdot \frac{1}{k_w} \tag{3.14}$$

SIFERRIT Materials

N 87

Relative core losses
versus AC field flux density
(measured on R34 toroids)

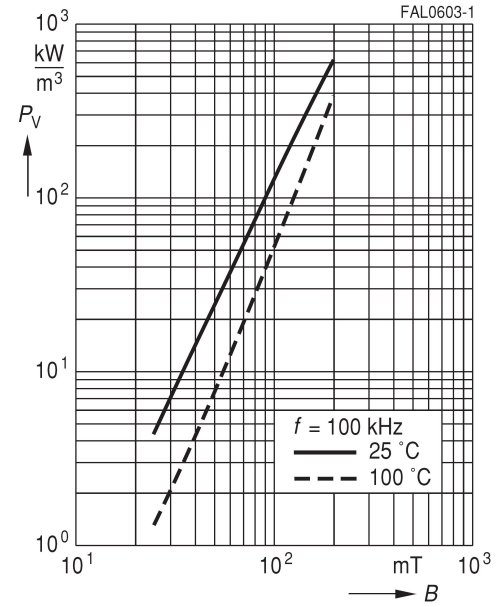

Relative core losses
versus temperature
(measured on R34 toroids)

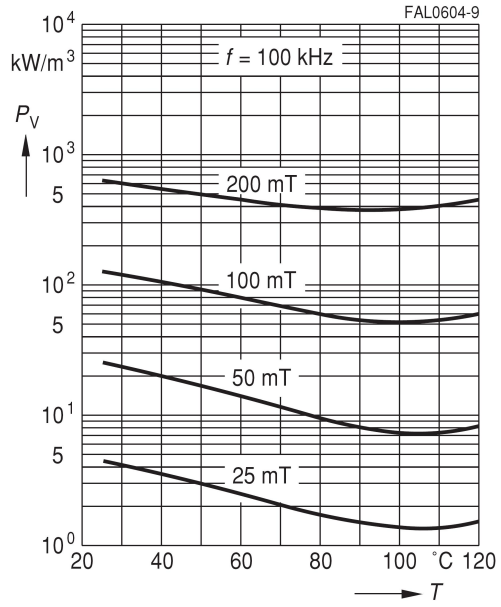

Relative core losses
versus frequency
(measured on R34 toroids)

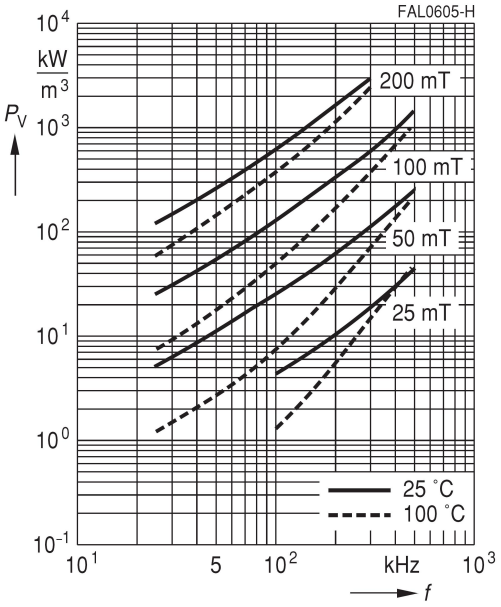

Figure 38: Power Losses diagrams (a) versus AC flux; (b) versus temperature; (c) versus frequency -provided from EPCOS data-sheet

E 25/13/7 (EF 25)

Core **B66317**

- To IEC 61246
- Delivery mode: single units

Magnetic characteristics (per set)

$\Sigma l/A$ = 1.1 mm^{-1}
l_e = 57.5 mm
A_e = 52.5 mm^2
A_{min} = 51.5 mm^2
V_e = 3020 mm^3

Approx. weight 16 g/set

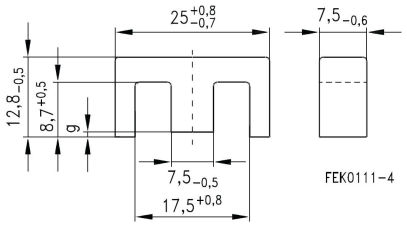

Coil former						Ordering code
Version	Sections	A_N mm^2	l_N mm	A_R value μΩ	Pins	
Horizontal	1	61	50	28	10	B66208B1110T001
Vertical	1	61	50	28	10	B66208X1010T001 B66208W1010T001
Yoke (ordering code per piece, 2 are required)						B66208A2010X000

Figure 39: Dimensions of single ferrite unit and the winding support relative to E25/13/7. A_N is the window area an l_N represent the average path of the winding.

Core Power losses

The maximal power allowed to be dissipated by the entire mutual inductor surface is 240mW, as explained in (3.4). In order to calculate the power dissipated in the core, it is useful to get the flux swing ΔB.

$$\begin{aligned}\Delta B &= \frac{\Delta\Phi}{A_e} = \frac{1}{A_e}\cdot\frac{L\cdot\Delta I}{N} = \frac{L\cdot I_{MAX}}{A_e\cdot N}\frac{\Delta I}{I_{Max}} \\ &= B_{MAX}\cdot\frac{\Delta I}{I_{MAX}} \\ &= 0,234T\cdot 0,15 = 35,1mT\end{aligned} \tag{3.15}$$

Where :

$$\Phi = \frac{N\cdot I}{\mathfrak{R}} = \frac{L\cdot I}{N} \tag{3.16}$$

The flux swing value calculated in (3.15) must be halved to find the power dissipated per unit of volume in figure 38 (because the reported data are referred to bipolar flux swing, and in flyback the flux is unipolar). Looking at the diagram of the relative core losses versus field flux density it is pointed out $P_V = 3\ kW/m^3$. So much less than the 100 mW/cm^3 rule of thumb that core losses are negligible, confirming that B_{MAX} is saturation limited at $I_{pk} = 1,05A$ [application notes Texas Instruments ANtexas pag 5-13]. Finally the total core losses are:

$$\begin{aligned}P_{diss}^{core} &= P_V \times Volume \\ &= 1,2\frac{kW}{m^3}\times 3020\cdot 10^{-9}m^3 \\ &\approx 3,6[mW]\end{aligned} \tag{3.17}$$

Improvement in temperature: $\Delta T = 10°C$

The thermal resistance of this core like in figure 40 is $R_{th} = 40[K/W]$; so the estimated total losses (core and winding) are: $P_t = \Delta T/R_{th} = 40/40 = 1[mW]$. Due to the small improve in the estimated temperature , it is possible to use the approximated formula (3.18), cited in [25] to guess the temperature rise of the transformer.

$$\Delta T = \frac{23.5 \cdot P_t}{\sqrt{AP}} = \frac{23.5 \cdot 240 \cdot 10^{-3}}{\sqrt{52,5 \cdot 10^{-2} \times 61 \cdot 10^{-2}}} \approx 10K \tag{3.18}$$

Using instead the more general formula and the value of $R_{th} = 46[K/W]$, that represents the thermal resistance of core and windings; from data sheet in figure 40 it can be found that:

$$\Delta T = R_{core} \times P_L = 40K \times 240 \cdot 10^{-3} \cong 9,6°K \tag{3.19}$$

The characteristic showed in figure 38, explain also that a eventual rise in temperature gives a lower power loss, so the temperature system can return back to his stable point.

3.1.3 *Air Gap*

In order to calculate the air gap, the energy density stored in the air gap has to be taken into account:

$$w = 1/2 \times B \times H = 1/2 \times \mu_0 \times H^2 \ [J/m^3] \tag{3.20}$$

where:

$\mu_0 = 4\pi \cdot 10^{-7}$ [H/m = V · s / A]

F = Magneto Motive Force [A]

H = Magnetic Field Intensity [A/m]

B = Magnetic Flux density [T=Wb/m^2]

w = energy density [J/m^3]

l = length of the magnetic path [m]

A = cross sectional area [m^2]

Within typical transformers, the magnetic energy is almost always confined to the regions where the field intensity H is almost constant and quite predictable. This often occurs in circuit winding as well [27]:

$$W = 1/2 \cdot \mu_0 \cdot H^2 \cdot A \cdot l \quad [J] \tag{3.21}$$

from Ampère's law, the total magneto motive force along any closed path of length l_e[m] that link together all N conductors:

$$mmF = \oint H dl = N \cdot I \qquad [J\ A] \tag{3.22}$$

6.6 Thermal resistance for the main power transformer core shapes

Core shapes	R_{th} (K/W)	Core shapes	R_{th} (K/W)	Core shapes	R_{th} (K/W)
RM 4	120	E 5	308	ER 9.5	164
RM 4 LP	135	E 6,3	283	ER 11/5	134
RM 5	100	E 8.8	204	ER 14.5/6	99
RM 5 LP	111	E 13/7/4	94	ER 28/17/11	22
RM 6	80	E 14/8/4	79	ER 35/20/11	18
RM 6 LP	90	E 16/6/5	76	ER 42/22/15	14
RM 7	68	E 16/8/5	65	ER 46/17/18	13
RM 7 LP	78	E 19/8/5	60	ER 49/27/17	9
RM 8	57	E 20/10/6	46	ER 54/18/18	11
RM 8 LP	65	E 21/9/5	59		
RM 10	40	E 25/13/7	40	ETD 29/16/10	28
RM 10 LP	45	E 25.4/10/7	41	ETD 34/17/11	20
RM 12	25	E 30/15/7	23	ETD 39/20/13	16
RM 12 LP	29	E 32/16/9	22	ETD 44/22/15	11
RM 14	18	E 32/16/11	21	ETD 49/25/16	8
RM 14 LP	21	E 34/14/9	23	ETD 54/28/19	6
		E 36/18/11	18	ETD 59/31/22	4
PM 50/39	15	E 40/16/12	20		
PM 62/49	12	E 42/21/15	19	EFD 10/5/3	120
PM 74/59	9,5	E 42/21/20	15	EFD 15/8/5	75
PM 87/70	8	E 47/20/16	13	EFD 20/10/7	45
PM 114/93	6	E 55/28/21	11	EFD 25/13/9	30
		E 55/28/25	8	EFD 30/15/9	25
EP 5	329	E 56/24/19	9.5		
EP 6	318	E 65/32/27	6.5	EV 15/9/7	55
EP 7	141	E 70/33/32	5.5	EV 25/13/13	27
EP 10	122	E 80/38/20	7	EV 30/16/13	21
EP 13	82	EI LP 14	116		
EP 17	58	EE LP 14	105	UU 93/152/16	4.5
EP 20	32	EI LP 18	61	UI 93/104/16	5
		EE LP 18	56	UU 93/152/20	4
P 9 × 5	142	EI LP 22	38	UI 93/104/20	4.5
P 11 × 7	106	EE LP 22	35	UU 93/152/30	3
P 14 × 8	73	EI LP 32	26	UI 93/104/30	4
P 18 × 11	51	EE LP 32	24	U 101/76/30	3.3
P 22 × 13	37	EI LP 38	20	U 141/78/30	2.5
P 26 × 16	27	EE LP 38	18		
P 30 × 19	22	EI LP 43	16		
P 36 × 22	17	EE LP 43	15		
		EI LP 58	12		
		EE LP 58	11		
		EI LP 64	9,5		
		EE LP 64	9		

Figure 40: Thermal resistance for the main power transformer core shape - Epcos data-sheets

Supposing that H is constant in all path, it is possible to substitute $H \cdot l = N \cdot I$:

$$W = 1/2 \cdot \mu_0 \cdot I^2 \cdot A/l \cdot N^2 \quad [J] \tag{3.23}$$

$$\begin{aligned} W &= 1/2 \cdot L \cdot I^2 \\ &= 1/2 \cdot \mu_0 \cdot N^2 \cdot A/l \cdot I^2 \quad [J] \end{aligned} \tag{3.24}$$

Supposing that all energy will stored in the air gap, and that the effect of fringing flux will be negligible; said l_{gap} the length of this region and supposing that this area will coincide with that one of the ferrite core inside the winding, from (3.24) it is obtained:

$$\begin{aligned} l_{gap} &= \frac{\mu_0 \cdot N^2 \cdot A_e}{L} \\ &= \frac{(4\pi 10^{-7} H/m) \cdot (35^2) \cdot (52,5\ 10^{-6} m^2)}{400 \cdot 10^{-6} H} \\ &\approx 0,2mm \end{aligned} \tag{3.25}$$

The nearest air gap values, available from data sheets, are: 0,15mm

Ungapped

Material	A_L value nH	μ_e	P_V W/set	Ordering code
N30	2900 +30/–20%	2530		B66317G0000X130
N27	1750 +30/–20%	1520	< 0.59 (200 mT, 25 kHz, 100 °C)	B66317G0000X127
N87	1850 +30/–20%	1620	< 1.60 (200 mT, 100 kHz, 100 °C)	B66317G0000X187

Gapped

Material	g mm	A_L value approx. nH	μ_e	Ordering code ** = 27 (N27) = 87 (N87)
N27, N87	0.10 ±0.02	489	425	B66317G0100X1**
	0.16 ±0.02	347	302	B66317G0160X1**
	0.25 ±0.02	250	218	B66317G0250X1**
	0.50 ±0.05	151	131	B66317G0500X1**
	1.00 ±0.05	91	79	B66317G1000X1**

The A_L value in the table applies to a core set comprising one ungapped core (dimension g = 0) and one gapped core (dimension $g > 0$).

Calculation factors (for formulas, see *"E cores: general information"*)

Material	Relationship between air gap – A_L value		Calculation of saturation current			
	K1 (25 °C)	K2 (25 °C)	K3 (25 °C)	K4 (25 °C)	K3 (100 °C)	K4 (100 °C)
N27	90	–0.731	139	–0.847	129	–0.865
N87	90	–0.731	139	–0.796	125	–0.873

Validity range: K1, K2: 0.10 mm < s < 2.00 mm
K3, K4: 60 nH < A_L < 570 nH

Figure 41: Table of inductance value for E25/13/7 gapped and ungapped core with N87 ferrite-Epcos Data sheets.

and 0,25mm (as provided in figure 41). corresponding to these two possibilities there are two possible solutions:

1- $l_{gap} = 0,15mm$, than the best trade off is obtained with
N=30, $B_{MAX} = 270mT$, $L = 396\mu H$, $\Delta I = 150mA$, $\Delta B = 40,5mT$

11- $l_{gap} = 0,25mm$, than the best trade off is obtained with
N=39, $B_{MAX} = 211mT$,L = $401\mu H$, $\Delta I = 150mA$, $\Delta B = 31,6mT$

It is chosen the first trade-off, because assure lower losses in the winding, since core losses are still low.

3.1.4 *Conductor sizing, winding resistance and losses*

Conductor sizing is guided from the power allowed to be dissipated on the winding.

Being $P_{diss}^{core} \approx 2,7mW$, as calculated in (3.17) and the entire power allowed to be dissipated in the entire mutual inductor (wire and core) $P_{diss}^{TOT} = 240mW$, it is possible to calculate the power that can be dissipated on the wire:

$$\begin{aligned} P_{diss}^{wire} &= P_{diss}^{TOT} - P_{diss}^{core} \\ &= 240 - 2,7mW = 237,3mW \\ &= (R_{dc} + R_{ac}) \cdot I^2 \end{aligned} \tag{3.26}$$

Given that the root mean square current through inductance is $I_{rms} = 0.719A$, as calculated in (3.3); and that $P_{diss}^{wire} = 237,3mW$, than:

$$R_{dc} + R_{ac} = \frac{P_{diss}^{wire}}{I^2} = \frac{237,3mW}{0,719^2\ A^2} \cong 459m\Omega \tag{3.27}$$

Furthermore, supposing that $R_{ac}/R_{dc} = 1,2$:

$$R_{dc} \cdot (1 + 1,2) \cong 459m\Omega \Rightarrow \quad R_{dc} = \frac{457mW}{2,2} = 208m\Omega \tag{3.28}$$

Being

$$\begin{aligned} A_{cu} &= \rho(100°C) \cdot \frac{N_{prim}}{R_{dc}} \cdot l_N \\ &= 23,1 \cdot 10^{-6}\Omega mm \cdot \frac{30}{208m\Omega} \cdot 50mm \\ &\cong 0,167mm^2 \rightarrow\ A_{cu} \geqslant \text{AWG } 24 \end{aligned} \tag{3.29}$$

Being AWG24 the minimal cross section allowed to be used in the winding; the window area, as declared in figure 39 is $A_w = 61mm^2$ where breadth is $b_w = 3,85$ mm; and width is $h_w = 15,3$ mm like in figure 43. In order to represent the loss of space due to the use of a round section wire instead of a square section one, it is introduced $K_{round} = (\pi/4) = A_{rnd}/A_{sq}$, where A_{round} represents the area of a round with 1mm ray and A_{sq} is the area of a square. A part of window area is occupied also by a creepage allowance M, that is necessary at each end of windings [26] pg 5-14. For this instance up to now it is supposed, $M = 0$.

The new available winding are is $A_{w_{free}} = b_w \times h_w = 15,3 \times 3,85 \approx 59mm^2$. The section area available for each cable can be calcu- *Choice of wire*

AMERICAN WIRE GAUGE DATA

AWG#	Bare area, 10^{-3} cm^2	Resistance, 10^{-6} Ω/cm	Diameter, cm
0000	1072.3	1.608	1.168
000	850.3	2.027	1.040
00	674.2	2.557	0.927
0	534.8	3.224	0.825
1	424.1	4.065	0.735
2	336.3	5.128	0.654
3	266.7	6.463	0.583
4	211.5	8.153	0.519
5	167.7	10.28	0.462
6	133.0	13.0	0.411
7	105.5	16.3	0.366
8	83.67	20.6	0.326
9	66.32	26.0	0.291
10	52.41	32.9	0.267
11	41.60	41.37	0.238
12	33.08	52.09	0.213
13	26.26	69.64	0.190
14	20.02	82.80	0.171
15	16.51	104.3	0.153
16	13.07	131.8	0.137
17	10.39	165.8	0.122
18	8.228	209.5	0.109
19	6.531	263.9	0.0948
20	5.188	332.3	0.0874
21	4.116	418.9	0.0785
22	3.243	531.4	0.0701
23	2.508	666.0	0.0632
24	2.047	842.1	0.0566
25	1.623	1062.0	0.0505
26	1.280	1345.0	0.0452
27	1.021	1687.6	0.0409
28	0.8046	2142.7	0.0366
29	0.6470	2664.3	0.0330

Figure 42: AWG diameters available; the first column provide the bare copper area, and the last one the external diameter. Table provided from constructor [39]

E 25/13/7 (EF 25)
Accessories **B66208**

Vertical version (B66208W, B66208X)

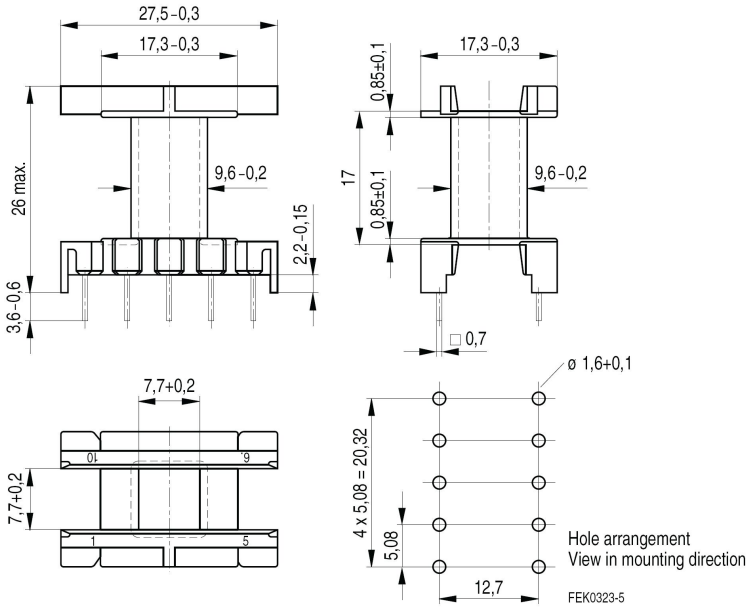

Figure 43: Dimensions of the coil former for EE25/13/7-Epcos Data-sheets

lated in this way:

$$A_{wire}^{available} = K_{round} \cdot \frac{A_{w_{free}}}{N_{prim} + N_{sec}}$$
$$\approx \frac{\pi}{4} \cdot \frac{59 mm^2}{60 \times 2}$$
$$\approx 0,7720 mm^2 \downarrow \quad (3.30)$$
$$A_{wire}^{available} \leqslant \text{AWG } 19 \quad (3.31)$$

Consequently to this result, the maximal wire available area is $A_{wire}^{available} = 0,772 mm^2$: the nearest value in the AWG table is represented by AWG 19 with a outside cross sectional area $0,7059 mm^2$. The wire can therefore be selected between AWG 24 and AWG 19. It is so selected AWG 20.

The copper temperature is supposed to be 100°C because it represents the worst-case; and the most likely case since the temperature in the winding is higher than 80°C. Recalculating R_{dc} with the new assumptions in cross sectional area AWG 20 (bare area $0,5188 = mm^2$, outside diameter$= 0,874 mm^2$):

$$R_{dc} = \rho(100°C) \cdot \frac{N_{prim} \cdot l_N}{A_{cu}}$$
$$= 23,1\ 10^{-6}\ \Omega mm \cdot \frac{30 \cdot 50\ mm}{0,5188\ mm^2}$$
$$\approx 66 m\Omega \quad (3.32)$$

Power dc losses are: *DC losses admitted*

Round Litz

Equivalent Gauge	Circular Mil Area	Number of Strands	Strand Gauge	Film Coating [1]	Construction Type	Outer Insulation [2]	Nominal Outside Diameter (inches)	Nominal LBS./MFT.	Direct Current Resistance OHMS/MFT.	Construction
Recommended Operating Frequency – 100 KHZ to 200 KHZ										
34	38.4	4	40	S	1	—	.008	.127	292.4	4/40
32	67.3	7	40	S	1	—	.011	.222	167.1	7/40
30	106.	11	40	S	1	SN	.017	.380	106.3	11/40
28	163.	17	40	S	1	SN	.020	.578	68.8	17/40
26	260.	27	40	S	1	SN	.024	.905	43.3	27/40
24	404	42	40	S	1	SN	.030	1.40	27.9	42/40
22	634.	66	40	S	2	SN	.040	2.23	18.2	3x22/40
20	1,036.	108	40	S	2	SN	.050	3.62	11.1	3/36/40
18	1,634.	170	40	S	2	SN	.061	5.67	7.05	5/34/40
16	2,595.	270	40	S	2	SN	.073	9.18	4.55	3/3/30/40
14	4,180.	435	40	S	2	SN	.093	14.8	2.83	5x3/29/40
12	6,727.	700	40	S	2	SN	.118	23.7	1.76	5x5x28/40
10	10,571.	1,100	40	S	2	SN	.148	37.3	1.12	5x5x44/40
8	17,298.	1,800	40	S	5	DN	.236	66.6	.700	6(5x3/20/40)
6	26,812.	2,790	40	S	5	DN	.293	103.	.451	6(5x3/31/40)
4	42,813.	4,455	40	S	5	SNB	.431	176.	.282	9(5x3/33/40)
2	69,192.	7,200	40	S	5	SNB	.572	290.	.174	12(5x3/40/40)
1/0	105,710.	11,000	40	S	5	SNB	.668	428.	.114	10(5x5x44/40)

Figure 44: Recommended number of strand in Litz wire provided by New England Wire Technology

$$P_{dc} = R_{dc} \times I_{rms}^2 \approx 66\ m\Omega \times 0,718^2\ A = 34\ mW$$

Penetration depth

Penetration depth at 100 kHz in a copper conductor , being ρ the copper resistivity at 100°C, can be calculated as [27]:

$$\delta_{pen} = \sqrt{\frac{\rho}{\pi \cdot \mu_0 \cdot f_{sw}}} = \sqrt{\frac{23,1 \cdot 10^{-9}}{\pi \cdot 4\pi 10^{-7} \cdot 100}} = 241,9 \tag{3.33}$$

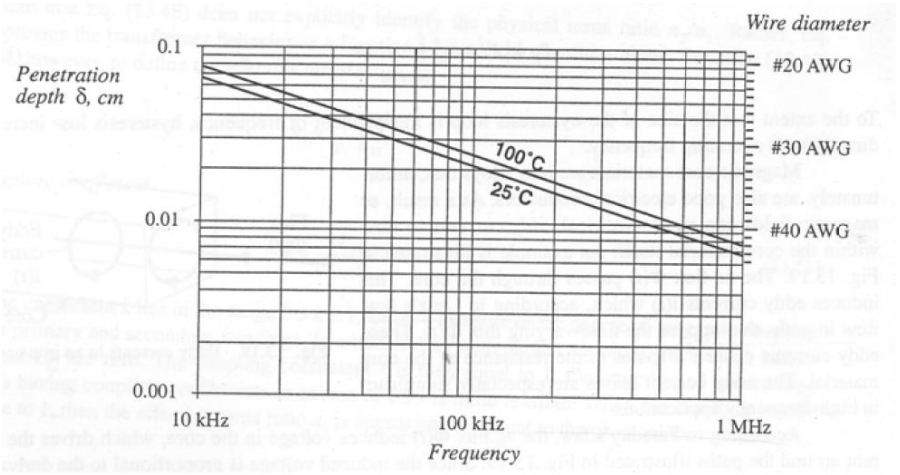

Figure 45: Penetration Depth provided from [39]. See also [25] pag 3.101 fig 3.4B.3

Let's call Q the ratio between Layer thickness and penetration depth; with an AWG 20 wire it is obtained the following value:

$$\begin{aligned} Q &= \frac{LayerThickness}{\delta_{pen}} \\ &= \frac{0,83 \cdot d_{cu} \cdot \sqrt{d_{cu}/s}}{\delta_{pen}} \\ &= \frac{0,83 \cdot 0,5188 \cdot 10^{-3} \cdot \sqrt{0,5188/0,874}}{241,9 \cdot 10^{-6}} \\ &= 1,37 \end{aligned} \tag{3.34}$$

Where Layer thickness $= 0,83 \cdot d_{cu} \cdot \sqrt{d_{cu}/s}$; d_{cu} is the diameter of the copper wire, and s is the center-to-center distance between wires [27]. Looking on figure 46 it is possible to notice that Q=1,37 (for two layers, because are supposed not interleaved) provide a $R_{ac}/R_{dc} \approx 2$: that means greater power losses (at least double), due to the skin effect. In order to reduce the skin effect, the diameter of the bare copper wire AWG 20 (0,5188mm) is compared with the penetration depth (0,242mm); it is possible to notice that at the frequency 100kHz the entire cross wire section is not used. This means that the skin effect is going to be relevant. To maintain a reasonable R_{ac}/R_{dc}, as assumed in (3.28), Litz wire with more strands of finer wire will be used. For this reason it is selected the Litz wire to use from tabel in figure 44: 108 strand where each strand is composed by wire AWG 40. The effect of this selection is evidenced by Dowell curves. Looking

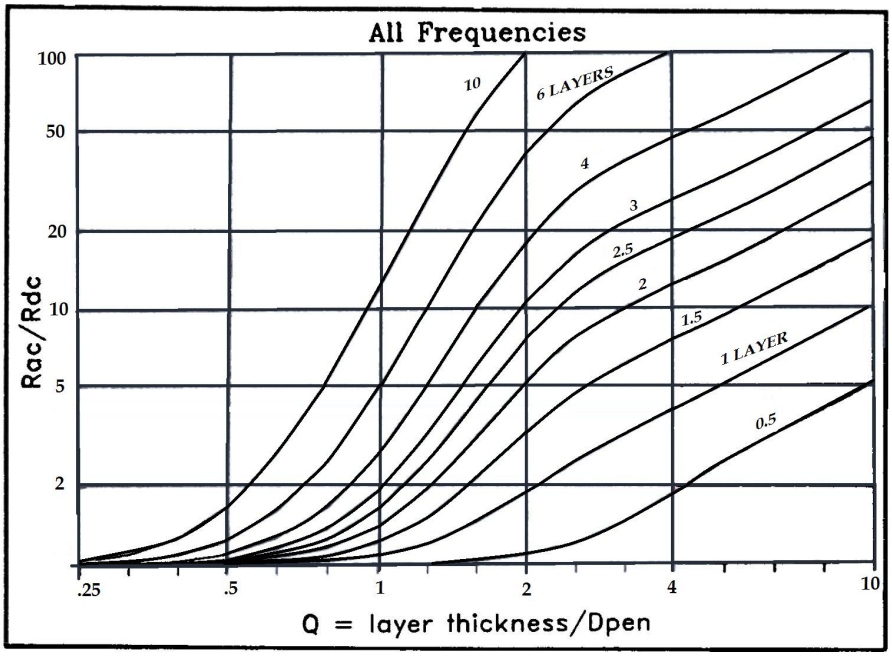

Figure 46: Dowell curves that represent the ratio between R_{ac}/R_{dc} versus $Q = layerthickness/D_{pen}$ these curves are valid only for sine wave inside the conductor, but will considered valid [27]

in figure 44, dimensions of AWG 40 are $A_{cu} = 0,0049mm^2$; $d_{cu} = 0,079mm$. The new value of Q has to be calculated again:

$$Q = \frac{LayerThickness}{\delta_{pen}} = \frac{0,83 \cdot d_{cu} \cdot \sqrt{d_{cu}/s}}{\delta_{pen}} = \frac{0,83 \cdot 0,079 \cdot 10^{-3}}{241,9 \cdot 10^{-6}} = 0,27 \tag{3.35}$$

The 108 strand of Litz wire can also be composed by 12 layers of 9 strand for each layer. In figure 46 it is pointed out that the new ratio $R_{ac}/R_{dc} \approx 1$.With this choice of litz wire, it will be $r_{dc} = 11,1 \cdot 10^{-3}\Omega/ft = 33,83 \cdot 10^{-3}\Omega m$, because (1ft=0,3048 m; and MFT= 1000 ft).

The new R_{dc} will be:

$$\begin{aligned} R_{dc} &= N \cdot l_N \cdot r_{dc} \\ &= 30 \cdot 50 \cdot 10^{-3} \cdot 33,83 \cdot 10^{-3} \\ &= 50,75m\Omega \end{aligned} \tag{3.36}$$

$$\begin{aligned} R_{ac} &= \frac{R_{ac}}{R_{dc}} \cdot R_{dc} \\ &= 1,2 \times 50,75 = 60,9m\Omega \end{aligned} \tag{3.37}$$

$$\begin{aligned} P^{wire}_{diss-prim} &= R_{dc} I^2_{rms} + R_{ac} I^2_{rms} = \\ &= 50,75 \cdot (1 + 1,2) \cdot 0,719^2 = 57,7mW \end{aligned} \tag{3.38}$$

$$P^{wire}_{diss-tot} = 2 \times P^{wire}_{diss-prim} = 115,4mW \tag{3.39}$$

The dissipated power on the entire mutual inductor (wire and core), remembering (3.17) and (3.39), should be:

$$P^{Tot}_{diss} = P^{wire}_{diss-tot} + P^{core}_{diss} = (115,4 + 3,6)\ mW = 119mW \tag{3.40}$$

3.2 WINDING DESIGN WITH INSULATION

In order to respect clearance distances, a thickness margin of 2mm is provided, so the length of the window for locating windings is 15,3mm-2mm= 11,3mm, so the new window area available for winding will be $A_w = b_w \times h_w = 3,65 \times 11,3 = 41,25mm^2$.

Supposing a raw of 15 wires, then the available external diameter is so calculated:

$$\begin{aligned} d^{ext}_{wire} &= h_w \div turns = 11,3 \div 15 \\ &= 0,753mm \rightarrow d_{wire} = 0,6426mm \end{aligned} \tag{3.41}$$

$$A_{cu} = 0,3243mm^2 \tag{3.42}$$

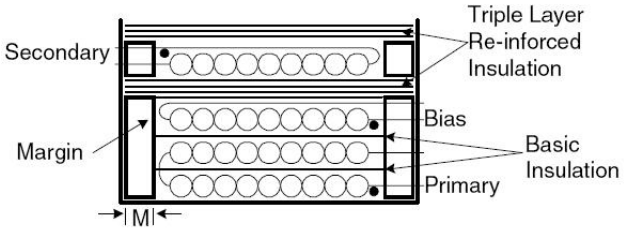

Figure 47: Margin wound transformer construction from [32]

$$A_{wire}^{available} = K_{round} \cdot \frac{A_w^{free}}{N_{prim} + N_{sec}}$$
$$\frac{\pi}{4} \cdot \frac{41,25}{60} \cong 0,54mm^2 \tag{3.43}$$
$$R_{dc} = \rho \cdot \frac{N \cdot l_N}{A_{cu}}$$
$$= 23,1 \times 10^{-6} \cdot \frac{30 \cdot 50}{0,3243}$$
$$\cong 107m\Omega \tag{3.44}$$

In order to calculate the ratio between R_{ac}/R_{dc}; Q is calculated as shown afterwards:

$$\tag{3.45}$$
$$Q = \frac{LayerThickness}{\delta_{pen}}$$
$$= \frac{0,83 \cdot d_{cu} \cdot \sqrt{d_{cu}/s}}{\delta_{pen}}$$
$$= \frac{0,83 \cdot 0,6426 \cdot 10^{-3} \cdot \sqrt{0,6426/0,701}}{241,9 \cdot 10^{-6}}$$
$$= 2,16 \tag{3.46}$$

With 1 layer, the corresponding value to $Q = 2,16$ is $R_{ac}/R_{dc} = 2,3$. In order to have an opportune ratio it is used Litz wire. The opportune value is selected looking in figure 44. The corresponding value to AWG 22 is 40 strand wire of AWG 40. With this value it is obtained $R_{ac}/R_{dc} = 1$. The new value of power dissipated in the primary will be:

$$P_{dc}^{prim} = (R_{dc} + R_{ac}) \times I_{rms}^2$$
$$= R_{dc} \cdot (1+1) \times I_{rms}^2$$
$$= 107m\Omega \cdot 2 \times 0,719^2 \cong 110,63mW \tag{3.47}$$

Primary and secondary windings have the same design parameters, than it is easy calculate the total dissipated power in the windings: $P_{wire}^{TOT} = 110,63 \times 2 \approx 222mW$ The total dissipated power will be:

$$P_{diss}^{TOT} = P_{wire}^{TOT} + P_{core}^{diss}$$
$$(222 + 3,6)mW = 224,8mW \tag{3.48}$$

3.3 WINDING SIZING RELAXING INSULATION RESTRICTIONS

It is possible try to relax the requirements about insulation. The meaning of Clearance and Creepage distances is here reported.

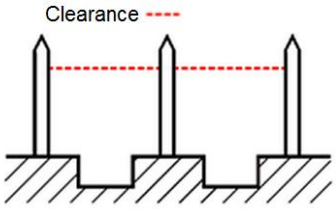

Figure 48: The clearance distance is defined as shortest distance thought the air between two conductive elements. [34]

Clearance (figure 48) is the shortest distance between two conductive parts, or between a conductive part and the bounding surface of the equipment, measured through air.

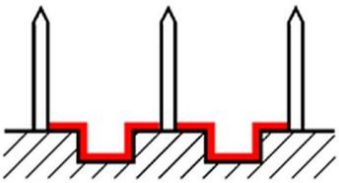

Figure 49: The creepage is defined as shortest distance on the surface the of an insulating material between two conductive elements [34].

Creepage (figure 49)distance is the shortest path between two conductive parts, or between a conductive part and the bounding surface of the equipment, measured along the surface of the insulation. All conductive parts are considered in evaluating the creepage distance, including parts around soldered connections.
The table in figure 50 reports the length of the creepage path. Based on this table an insulating thickness of 1mm is selected. In this way the creepage path will be 2mm long.

The new value of the available window will be: $15,3mm - 2mm = 13,3mm$

$$\begin{aligned} d_{wire}^{ext} &= h_w/\text{turns per layer} = 13,3/15 \\ &= 0,8867mm \rightarrow AWG20\ d_{wire} = 0,874mm\ A_{cu} = 0,5188mm^2 \end{aligned} \tag{3.49}$$

$$\begin{aligned} R_{dc} &= \rho \cdot \frac{N \cdot l_N}{A_{cu}} \\ &= 23,1\ cdot10^{-6}\frac{30 \cdot 50}{0,5188} \\ &\cong 67m\Omega \end{aligned} \tag{3.50}$$

In order to calculate the ratio between R_{ac}/R_{dc}; Q it is calculated

$$Q = \frac{LayerThickness}{\delta_{pen}} = \frac{0,83 \cdot d_{cu} \cdot \sqrt{d_{cu}/s}}{\delta_{pen}} = \frac{0,83 \cdot 0,813 \cdot 10^{-3} \cdot \sqrt{0,813/0,874}}{241,9 \cdot 10^{-6}} \approx 2,7 \tag{3.51, 3.52}$$

	Funtional, Basic, and Supplementary Insulation							
Working Voltage V Rms or Dc	Pollution Degree 1	Pollution Degree 2			Pollution Degree 3			
	Material Group	Material Group			Material Group			
	I, II, IIIa, or IIIb	I	II	IIIa, or IIIb	I	II	IIIa, or IIIb
<50	Use the clearance from the appropriate tables	0.6	0.9	1.2	1.5	1.7	1.9
100		0.7	1.0	1.4	1.8	2.0	2.2
125		0.8	1.1	1.5	1.9	2.1	2.4
150		0.8	1.1	1.6	2.0	2.2	2.5
200		1.0	1.4	2.0	2.5	2.8	3.2
250		1.3	1.8	2.5	3.2	3.8	4.0
300		1.6	2.2	3.2	4.0	4.5	5.0
400		2.0	2.6	4.0	5.0	5.6	6.3
600		3.2	4.5	5.3	8.0	9.5	10.0
800		4.0	5.6	8.0	10.0	11.0	12.5
1000		5.0	7.1	10.0	12.5	14.0	16.0
Linear interpolation is permitted between the nearest two points, the calculated spacing being rounded to the next higher 0.1-mm increment.								

Table IV. Table 2L of the standard provides minimum creepage distances (creepage distances in millimeters).

Figure 50: Table of Creepage distances

Supposing to interleave only one layer between primary and secondary, the corresponding value to Q=2,7 is $R_{ac}/R_{dc} \approx 3$. To choose the Litz wire, the opportune value is selected from figure 44. The corresponding value to AWG 20 is composed by 108 strands of AWG 40 wires. Than $R_{ac}/R_{dc} = 1$ is obtained. The new value of power dissipated in the primary will be:

$$\begin{aligned} P_{dc}^{prim} &= (R_{dc} + R_{ac}) \times I_{rms}^2 \\ &= R_{dc} \cdot (1+1) \times I_{rms}^2 \\ &= 67m\Omega \cdot 2 \times 0,719^2 \cong 70mW \end{aligned} \tag{3.53}$$

Having primary and secondary the same design, it is easy calculate the total dissipated power in the windings: $P_{wire}^{TOT} = 70mW \times 2 \approx 140mW$

The total dissipated power will be:

$$\begin{aligned} P_{diss}^{TOT} &= P_{wire}^{TOT} + P_{core}^{diss} \\ &(140 + 3,6)mW \approx 144mW \end{aligned} \tag{3.54}$$

Enough to ensure the required efficiency.

4

BIDIRECTIONAL FLYBACK AS PROPOSED CHARGE EQUALIZER

4.1 ANALYSIS AND SIMULATION

Here a charge equalizer based on bidirectional flyback topology is proposed, in order to enable the energy flux in both directions. The aim of this circuit is indeed to equalize two neighbouring batteries when those are unbalanced. The transformer is needed to provide the galvanic insulation among batteries. In steady state with a Duty cycle D = 50% (the duty cycle is defined as $D = t_{sw1}/T_{SW}$ when t_{sw1} is the time during the switch is "on" and Tsw is the switching time and the duty cycle is related to the switch SW1) all charge taken out from battery B1 (the chargest one) has to be moved to the weakest battery B2, through the mutual inductor.

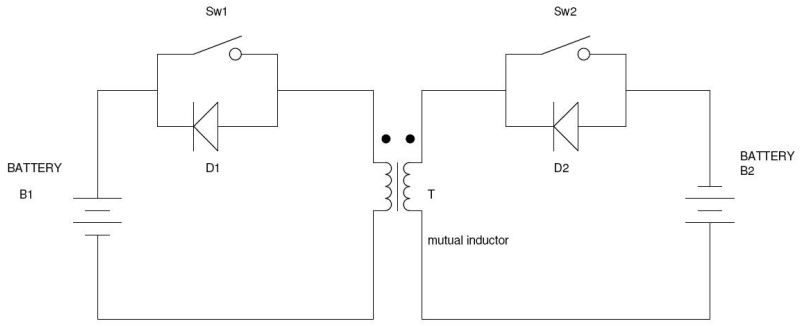

Figure 51: Dual flyback: topology proposed as charge equalizer

4.2 ANALYSIS OPEN LOOP OF THE BI-DIRECTIONAL FLYBACK

To transfer energy from battery B_1 to battery B_2, the involved switches are sw_1 (active) and D_2 (passive) as showed in figure 52. In figure 53, the mutual inductor is modellized as ideal. This model is composed by current controlled generators, in order to provide the characteristic relationship between input/output currents and voltages of the mutual inductor. It only uses current controlled generators, because the voltage generators in this circuit with LT Spice cause some convergence problems. In order to modelize the voltages, a resistor R1 is placed inside the model. Due to the bidirectionality, the mutual inductor must be symmetric, and consequently the turns ratio of the transformer has to be one. In figure 54 and 55 the currents and voltages incoming and outcoming the transformer when duty cycle is 50% are represented. To proof that the energy flux flows from B1 to B2, in figure 57 it can easily noticed that the current is outgoing from battery(is positive)

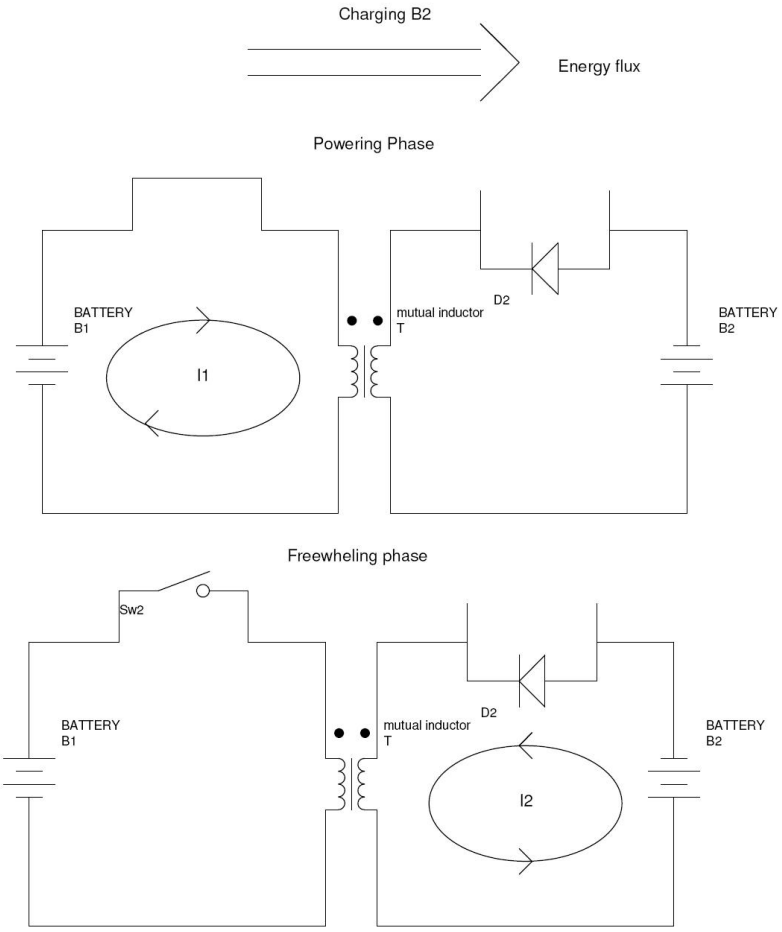

Figure 52: Energy flux from B_1 to B_2. It is evedenced how the currents are handled by the switches.

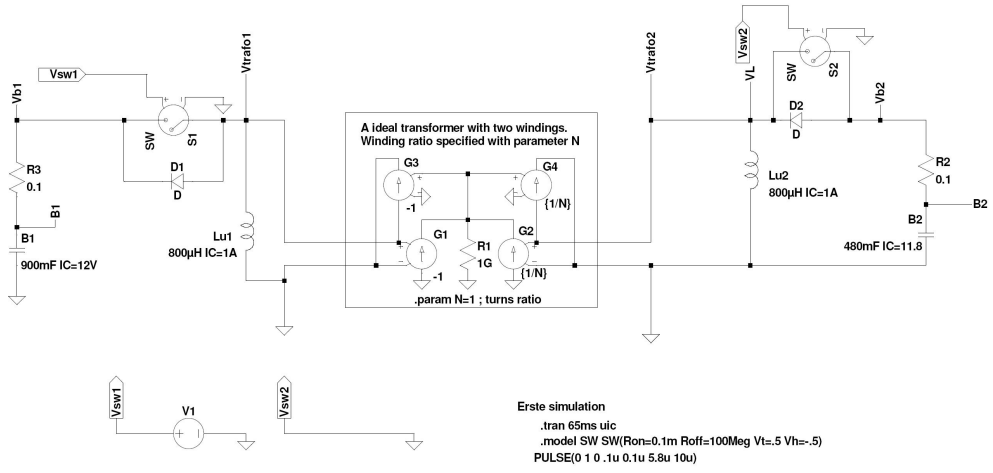

Figure 53: Schematics used for simulation open loop

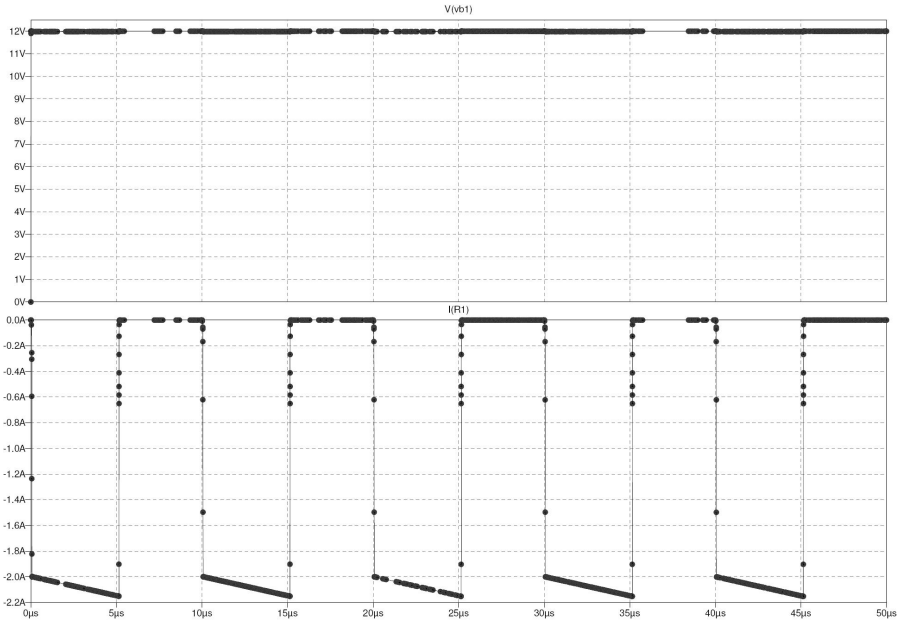

Figure 54: In this figure are rappresented: the voltage between the battery: V(b1) the battery with more charge b1, , and I(R3) the incoming current ViB1

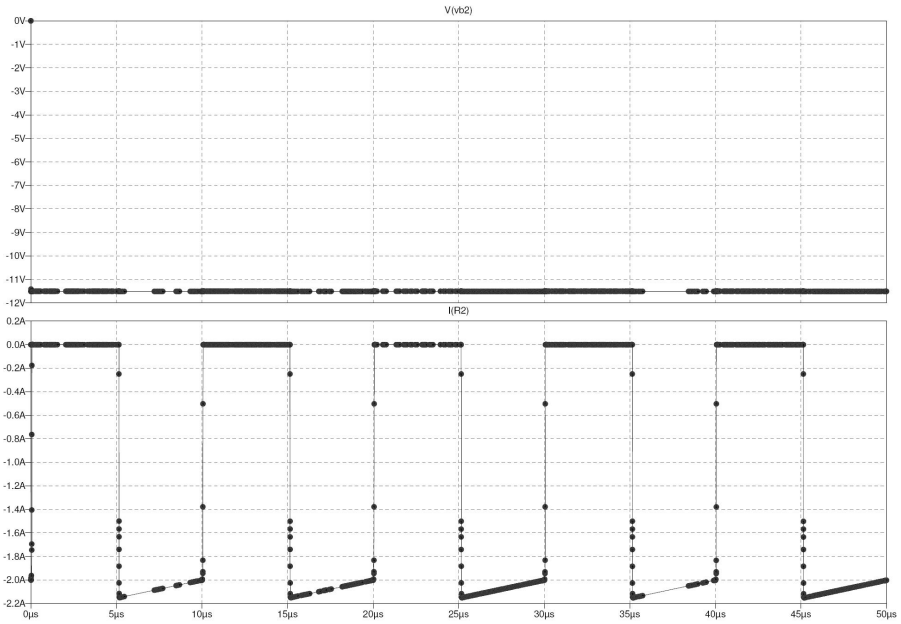

Figure 55: V(b2) the opposite coltage of the weakest battery b2, I(R2) the outgoin current

In figure 54 are depicted the voltage of B1 and the incoming current (that is negative). That means that there is an outcoming energy flux, that is provided to the weakest battery. In figure 55 are depicted the voltage of the battery B2 and the incoming current: both are negative, that means the energy flux is incoming in the battery and it is going to be charged.

4.3 DESIGN OF CURRENT CONTROL

An average current control was choosen in order to have a better control. Because it is planned to work all the time in CCM (Continous Conduction Mode), the current through the inductance will be not so far away from the average value. To accomplish this control, a small signal model of the converter is needed. The Assuming that Bidirectional Flyback transfer energy from battery B_1 to B_2, than it can simplified as a Buck-Boost equivalent circuit. To design the control system it is necessary develop the small signal model of the switching cell.

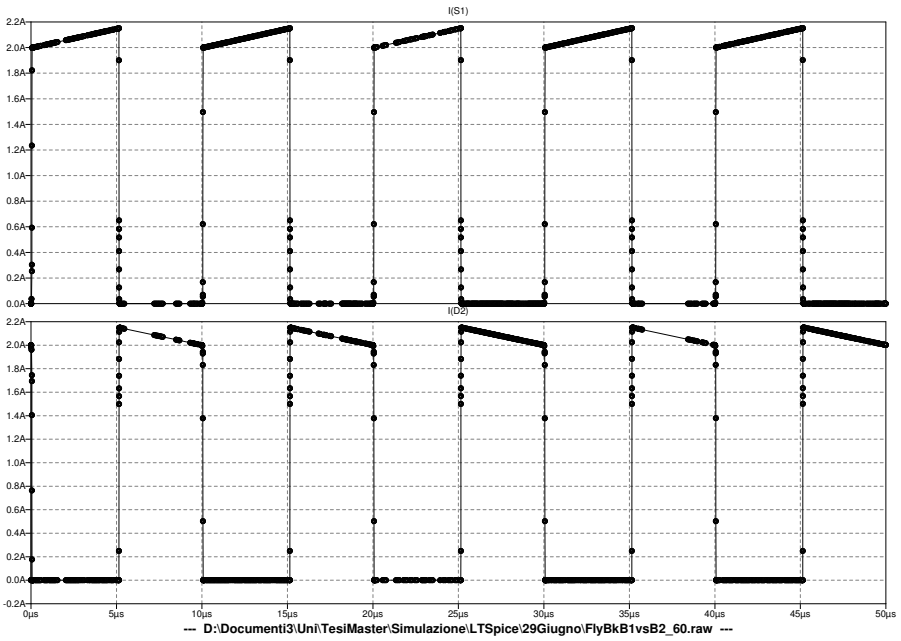

Figure 56: Current trough switch S1 and through diode D2

4.4 CONTROL DESIGN

The control of the charge equalizer will be composed by a current control loop , and a voltage control loop. In order to design the right control system, an average and equivalent ideal model is done.

The linearized model can be perturbed to find a dynamic model: The equations that resume the behaviour of the system are depicted in figure 59 and are presented here below, where $S = j\omega$ and $\omega = 2 \cdot \pi \cdot f$ [rad/s] is the angular frequency:

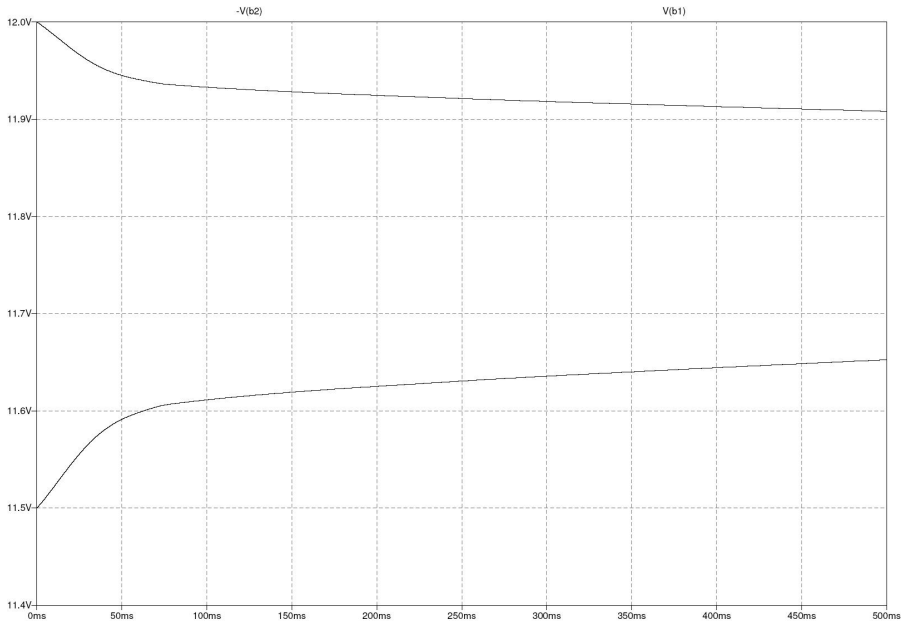

Figure 57: It is evidenced that the voltage of the weakest battery rise-up, and approach to the the voltage of the battery B2 that felt down.

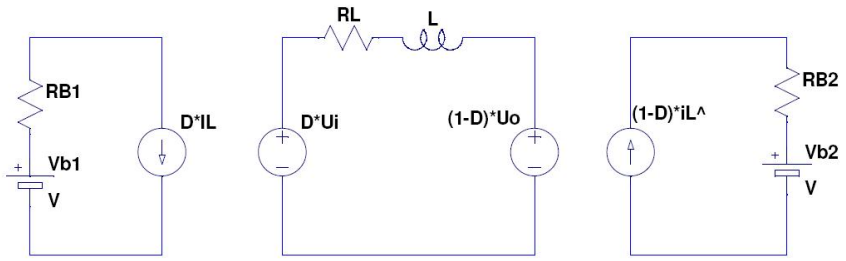

Figure 58: Average model of the Buck-boost equivalent to the Flyback applyied to the easiest Battery model ([40])

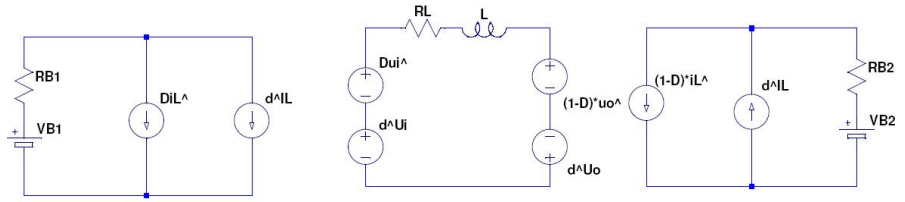

Figure 59: Buck-boost converter small-signal ac equivalent model supposing to modelize the battery with an Ideal Battery cell and a resistor(pag 212 [39])

$$\widehat{i_L} = \left(D\ \hat{u}_i + U_i\ \hat{\delta} + U_o\ \hat{\delta} - (1-D)\ \widehat{u_o}\right) \cdot \left(\frac{1}{R_L + S\ L}\right) \tag{4.1}$$

$$\widehat{u_o} = \left(V_{B_2} + ((1-D) \cdot \widehat{i_L} - I_L\ \hat{\delta})\right) \cdot R_{B_1} \tag{4.2}$$

$$\widehat{u_i} = \left(V_{B_1} - (I_L\ \hat{\delta} + D\ \widehat{i_L})\right) \cdot R_{B_1} \tag{4.3}$$

Where $\widehat{i_L}$ $\widehat{u_o}$ and $\widehat{u_i}$ are the variations of the current through the inductance, variations of the "output voltage" (or week battery B2) and variations of the "surce battery"(or the more charged battery B1). In order to obtain a transfer function between the current through inductance (the controlled value) and duty cycle (controlling value), it is substituted (4.2) in (4.1) and is obtained:

$$\begin{aligned} &\widehat{i_L} \cdot \left[D^2 \cdot R_{B_2} + D'^2 \cdot R_{B_1} + R_L + S\ L\right] \\ &= \hat{\delta} \cdot \left[U_i + U_o - D\ R_{B_2}\ I_L + D'\ R_{B_1}\ I_L\right] \end{aligned} \tag{4.4}$$

The transfer function between the duty cycle and the current is shown in (4.5). Because of the small size of R_B (resistance battery), and because of the fact that the duty cycle is smaller than one ($0.5 < D < 1$), the contribute of $D^2\ R_{B_1}$ and $D^2\ R_{B_2}$ can be neglected in comparison with R_L, because it is at least 100 times smaller.

$$G_{i\delta}(s) = \frac{\widehat{i_L}}{\widehat{\delta}} = K_{i\delta} \cdot \left(\frac{1}{1 + s \cdot \frac{L}{R_L + D^2\ R_{B_2} + D'^2\ R_{B_1}}}\right) \tag{4.5}$$

$$\approx \frac{k_{i\delta}}{1 + s\ \frac{L}{R_L}} = \frac{120}{1 + \frac{s}{500}} \tag{4.6}$$

where the value of $K_{i\delta}$ can be calculated like:

$$K_{i\delta} = \frac{U_i + U_o + I_L\ (R_{B_1}\ D' - R_{B_2}\ D)}{R_L^* + D^2\ R_{B_2} + D'^2\ R_{B_1}} \tag{4.7}$$

$$\approx \frac{U_i + U_o}{R_L^*} = \frac{24V}{200\ m\Omega} = 120A \tag{4.8}$$

The current-duty cycle transfer function $G_{i\delta}$ is depicted by Matlab in figure 60

Here are figure **[?]** the Bode Plot of the function $G_{i\delta}$ (4.5) obtained with Matlab.

The duty cycle is determinate by a PWM technique, that compares a sawtooth signal with a modulating signal u_m, proportional to the current error. This signal is composed by an average value and an oscillating part proportional to the current ripple through the inductance [40] [38], just inverted because of the difference in the reference of the signal (in figure 66 called also *vIref*). Being u_m the output signal of the regulator, its dynamic is a direct consequence of the regulator's transfer function. As consequence of this swing, the intersection point can vary accordingly to this swing, as well as the duty cycle.

$$\delta = \frac{1}{A_w \left(1 + \frac{\bar{m_1}}{2\ f_{sw}} \cdot \frac{R_S\ K_p}{A_w}\right)} \cdot \bar{u_m} \tag{4.9}$$

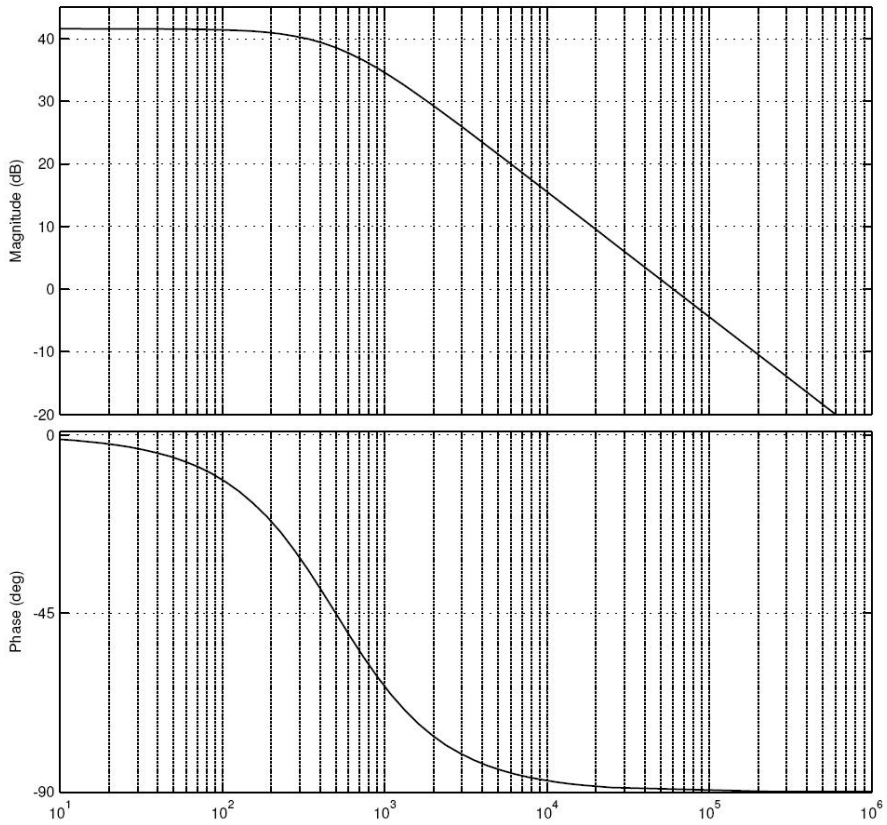

Figure 60: Bode plot of the transfer function $G_{i\delta}(s)$ it evidence the pole at angular frequency $\omega = 500$ rad/s and the magnitude at low frequency ($G_{i\delta}(0)$=41.6 dB)

When $\bar{u_m}$ is the average value of u_m. This formula results recognizing that:

$$\bar{u_m} - s_1 \frac{t_{on}}{2} = \frac{A_w}{T_{sw}} \cdot t_{on} \tag{4.10}$$

in the hypothesis that the regulator influences the slope of the current error, only the coefficient K_p has to be taken into account, you obtain

$$\bar{u}_m - \bar{m}_1 \, R_s \, K_p \frac{t_{on}}{2} = A_w \, \delta \tag{4.11}$$

and then results (4.9)

The duty cycle's variation depends on the u_m, u_o and u_i variations: indeed the variations of the slope m1 and m2 are determined by the variations of the voltages u_o and u_i.

$$\begin{aligned} \hat{\delta} &= \frac{\partial \delta}{\partial u_m} \widehat{u_m} + \frac{\partial \delta}{\partial m_1} \frac{\partial m_1}{\partial u_o} \widehat{u_o} + \frac{\partial \delta}{\partial u_m} \frac{\partial u_m}{\partial u_i} \widehat{u_i} \\ &= h_{\delta m} \widehat{u_m} + h_{\delta u_o} \widehat{u_o} + h_{\delta u_i} \widehat{u_i} \end{aligned} \tag{4.12}$$

The coefficient of each contribute's variation are presented here:

$$h_{\delta m} = \frac{\partial \delta}{\partial u_m} = \frac{1}{A_w \left(1 + \frac{\bar{m}_1}{2 \, f_{sw}} \frac{R_s \, K_p}{A_w}\right)} \tag{4.13}$$

$$h_{\delta u_i} = \frac{\partial \delta}{\partial u_i} = \frac{1}{A_w \left(1 + \frac{\bar{m}_1}{2 \, f_{sw}} \frac{R_s \, K_p}{A_w}\right)^2} \cdot \frac{R_s \, K_p}{2 \, L \, f_{sw}} \tag{4.14}$$

Assuming that the variations of the batteries' voltage have got negligible impact on the duty cycle variation, $h_{\delta u_i}$ and $h_{\delta u_o}$ can be considered zero. As depicted by figure 61, the current error is sensed

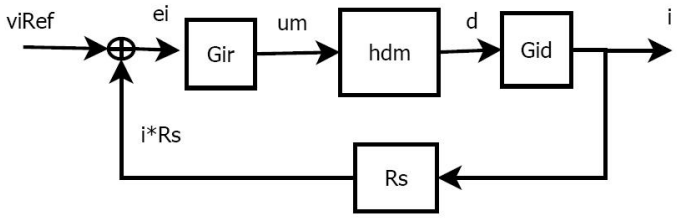

Figure 61: Block scheme relative to Current Loop. Are showed:
G_{ir}, current regulator;
h_{dm}, modulator's transfer function;
G_{id}, transfer function representative of the buck-boost duty cycle (input)-current through inductance(output);
R_s, sensing resistor.

through R_s. This ripple is inverted (due to the difference with the current reference), and the inductor current downslope becomes an upslope ([38] page 3-358). As regulator, a proportional-integral network as regulator is used:

$$G_{ri}(s) = K_P + \frac{K_I}{s} \tag{4.15}$$

the u_m slope can be calculated by starting the current ripple slope, and supposing that in the involved frequency range (at the ripple frequency) the integral part has no influence:

$$s_1 = m_1 \cdot R_s \cdot K_P \tag{4.16}$$

$$s_2 = m_2 \cdot R_s \cdot K_P \tag{4.17}$$

The hypothesis above can be verified by looking at figure 63: only at 100kHz the integral part has no effect anymore. To avoid sub-harmonic oscillation (static instability), the slope s_2 must not exceed the oscillator ramp slope. On the other side, the slop s_2 must be as big as possible, in order to have an optimum gain ([38] page 3-358). For this reason, supposed to be A_w the peak value of the sawtooth, it is important respect this relation:

$$s_2 \leqslant \frac{A_w}{T_{sw}} \rightarrow m_2 \; R_s \; K_p \leqslant A_w \; f_{sw} \tag{4.18}$$

that can also be written:

$$k_p \leqslant \frac{A_w \; F_{sw}}{m_2 \; R_s} \tag{4.19}$$

Assuming that $h_{\delta u_i}$ and $h_{\delta u_o}$ are zero, and that $G_{i\delta}$ can be approximated like an ideal integrator (the frequency range involved is as close as possible to the switching frequency, and consequently the pole frequency of $G_{i\delta}$ is well below and for this reason can be neglected); furthermore the gain's regulator (k_p) can be supposed to be constant in the frequency range involved, the loop gain can be calculated like:

$$T_i = G_{i\delta} \cdot G_{R_i} \cdot R_s \cdot h_{\delta u_n} \tag{4.20}$$

$$\approx \frac{K_{i\delta}}{s \; \frac{L}{R_L^*}} \cdot K_P \cdot R_S \cdot h_{\delta u_m} \tag{4.21}$$

Analyzing the last part of the equivalence, it is obtained:

$$R_s \cdot K_p \cdot h_{\delta u_m} = R_s \; K_p \; \frac{1}{A_w \cdot \left(1 + m_1 \; \frac{R_s \; K_P}{2 f_{sw} \; A_w}\right)}$$

$$= \frac{2 f_{sw}}{2 \cdot \frac{f_{sw} A_w}{R_s K_p} + m_1} \tag{4.22}$$

$$\tag{4.23}$$

where the last equivalence is true if considered that to avoid instability problems must be respected equation (4.19). In order to get the optimal gain and to respect the limit on K_p represented in equation (4.19) it is imposed that $m_2 = \frac{f_{sw} A_w}{K_P R_s}$, and obtained that:

$$R_s \cdot K_p \cdot h_{\delta u_m} = \frac{fsw}{2m_2 + m_1} \tag{4.24}$$

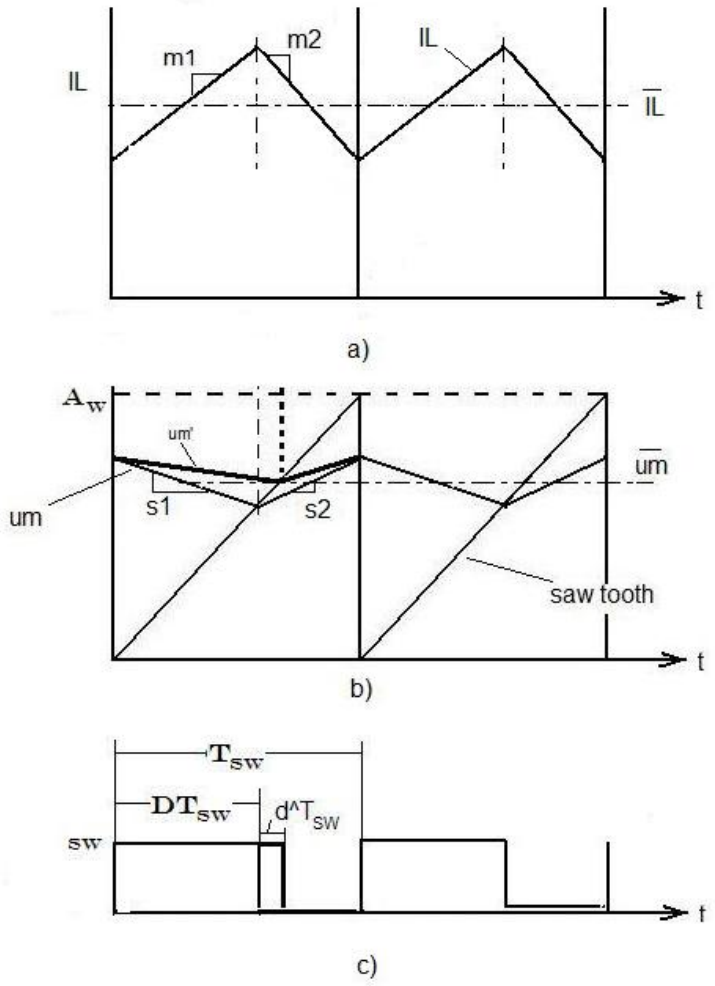

Figure 62: This picture represent:
a) Current thought the inductance;
b) oscillating saw tooth signal, and um signal and a hypothetical variation of u_m slope (m1) that cause a variation on duty cycle value;
c) SW is a logic signal that turn the switch on if hight.

For this reason can be also:

$$|T_i(s)| \leqslant \left| \frac{K_{i\delta}}{s\ L/R_L^*} \right| \cdot \frac{2f_{sw}}{2m_2 + m_1}$$

remembering that $m_2 = \frac{U_o}{L}$ and $m_1 = \frac{U_i}{L}$

$$\leqslant \left| \frac{K_{i\delta}}{s\ \frac{L}{R_L^*}} \right| \cdot \frac{2f_{sw}}{\frac{U_i + 2\ U_o}{L}} \tag{4.25}$$

Where D is duty cycle, D'=1-D, and $\frac{U_o}{U_i} = \frac{D}{1-D} = \frac{D}{D'}$. Reminding that $k_{i\delta} \approx \frac{U_i + U_o}{R_L^*}$, it is obtained

$$1 = |T_i(2\pi f_c)| \leqslant \frac{\frac{U_i + U_o}{R_L^*}}{2\pi f_c\ \frac{L}{R_L^*}} \cdot \frac{2f_{sw}}{\frac{U_i + 2\ U_o}{L}} \tag{4.26}$$

The value of the cross frequency is determined by

$$f_c \leqslant \frac{f_{sw}}{\pi\ (1 + D)} \tag{4.27}$$

This upper bound is consequently determined by the Duty cycle value, that in the worst case (lower upper bound) is $D = 1$, than it follows:

$$f_c \leqslant \frac{f_{sw}}{2\ \pi} = \frac{100\text{kHz}}{2\ \pi} \approx 16\text{kHz} \tag{4.28}$$

$$\omega_c \leqslant 10^5 \text{rad/s} \tag{4.29}$$

The maximum proportional gain of the regulator is calculated assuming, that $A_W = 1V; R_S = 1\Omega$; it is obtained: *calculation of* K_P

$$K_p \leqslant \frac{A_w\ f_{sw}}{m_2\ R_s} = \frac{A_w\ f_{sw}}{U_o} \cdot \frac{L}{R_s} = \frac{10V \cdot 100\text{kHz}}{12V} \frac{400\mu\text{H}}{1\Omega} \approx 30\ V \tag{4.30}$$

In figure 60 the Bode plot of the transfer function control (duty cycle-current through the inductance) $G_{i\delta}$ and the transfer function of the current regulator are presented G_{ri} in figure 63 both obtained using Matlab.

In figure 64 is depicted the current loop transfer function T_i as described in formula (4.21) here reported:$T_i = G_{i\delta} \cdot G_{Ri} \cdot h_{\delta u_m}$ (it must be noticed that $h_{\delta\ u_m} \approx 1/10$ because $A_w = 10V$). The entire bode plot of the closed loop system is presented in figure 65. In figure 66 a schematic of a Buck-boost equivalent to the Flyback system is presented. The switch is replaced by an ideal switch; a voltage current controlled source "H_1" is used to get a voltage measure proportional to the current through the inductance "i_L". The Current loop compensator is composed by an ideal operational amplifier (voltage controlled source with high

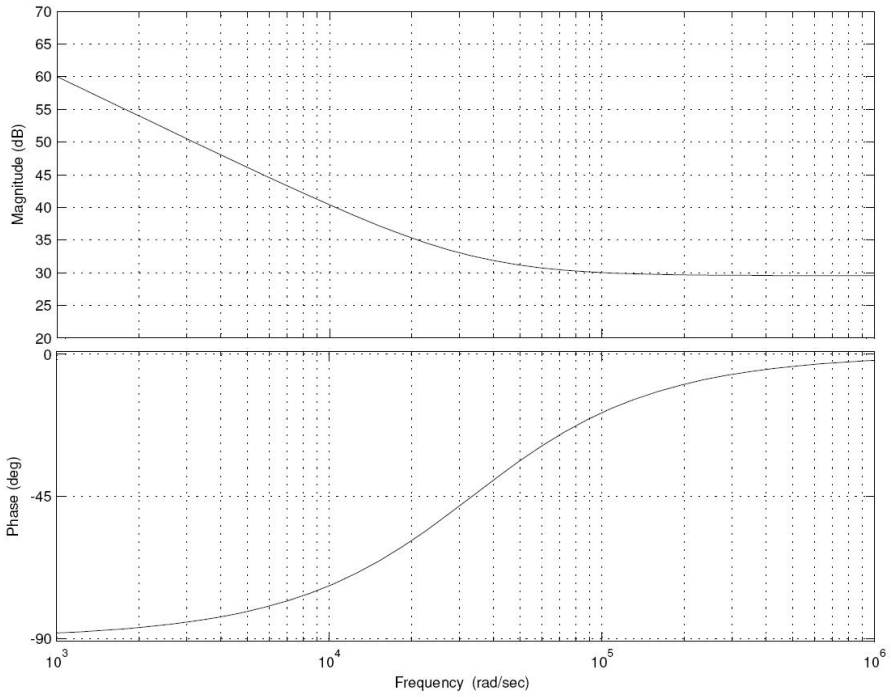

Figure 63: Bode Current Regulator transfer function G_{ri}

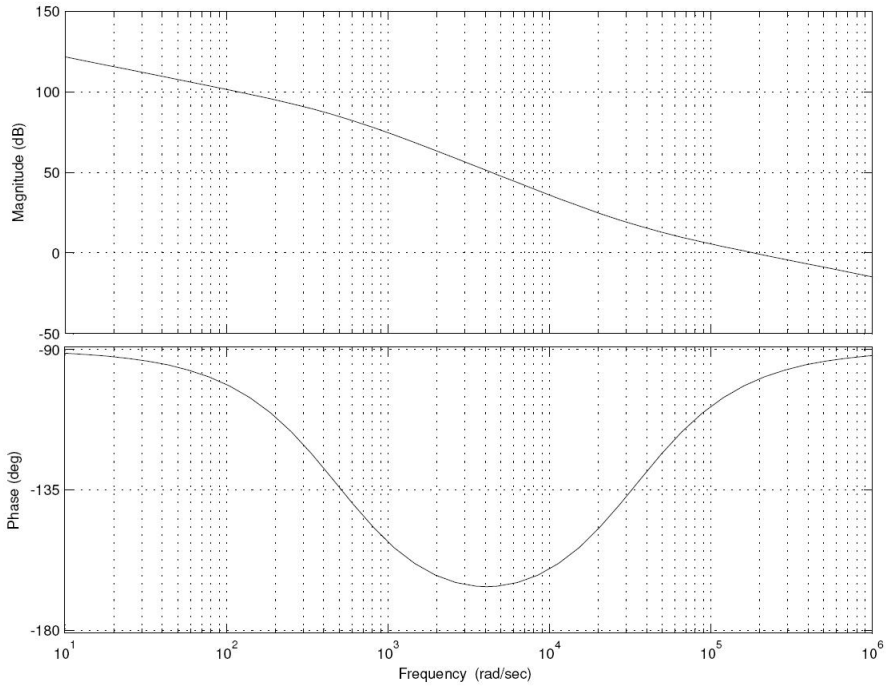

Figure 64: Current loop gain T(j ω)

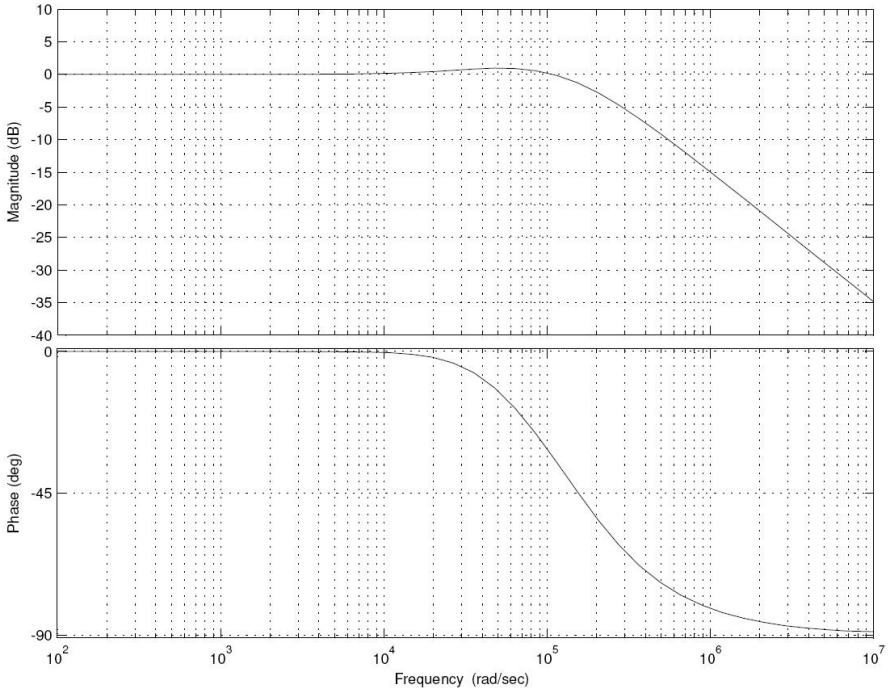

Figure 65: Bode Plot of the entire closed loop sistem

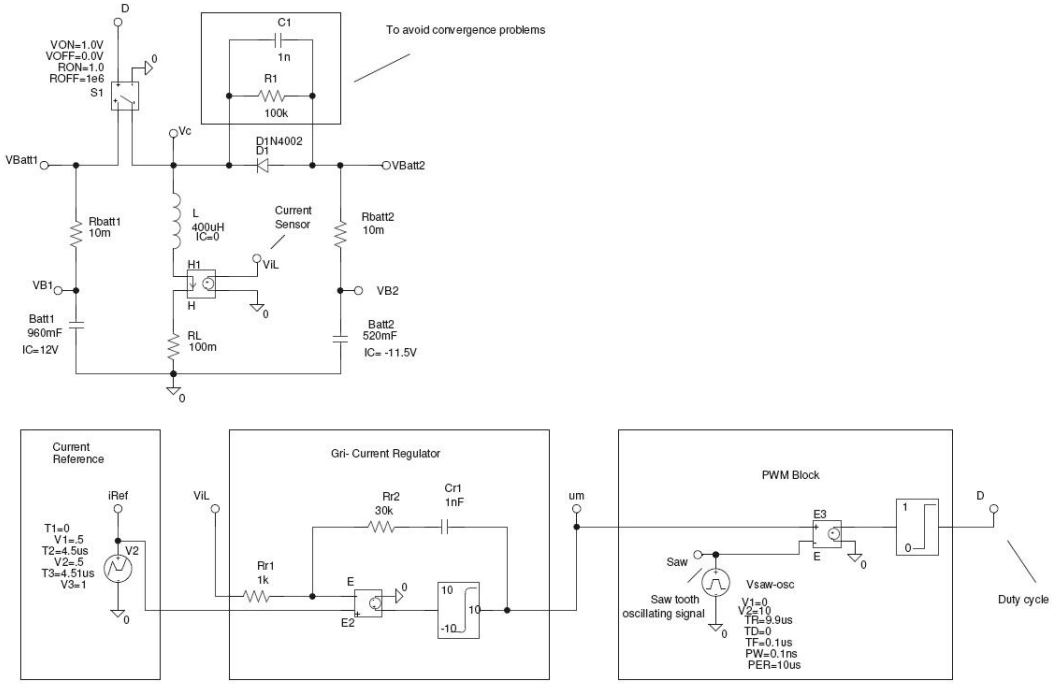

Figure 66: Schematics of the Buck-boost equivalent: Current control with ideal-equivalent OpAmp model.
(iRef) is the voltage signal proportional to the current reference,
(ViL) is the voltage proportional to the current through the inductance.

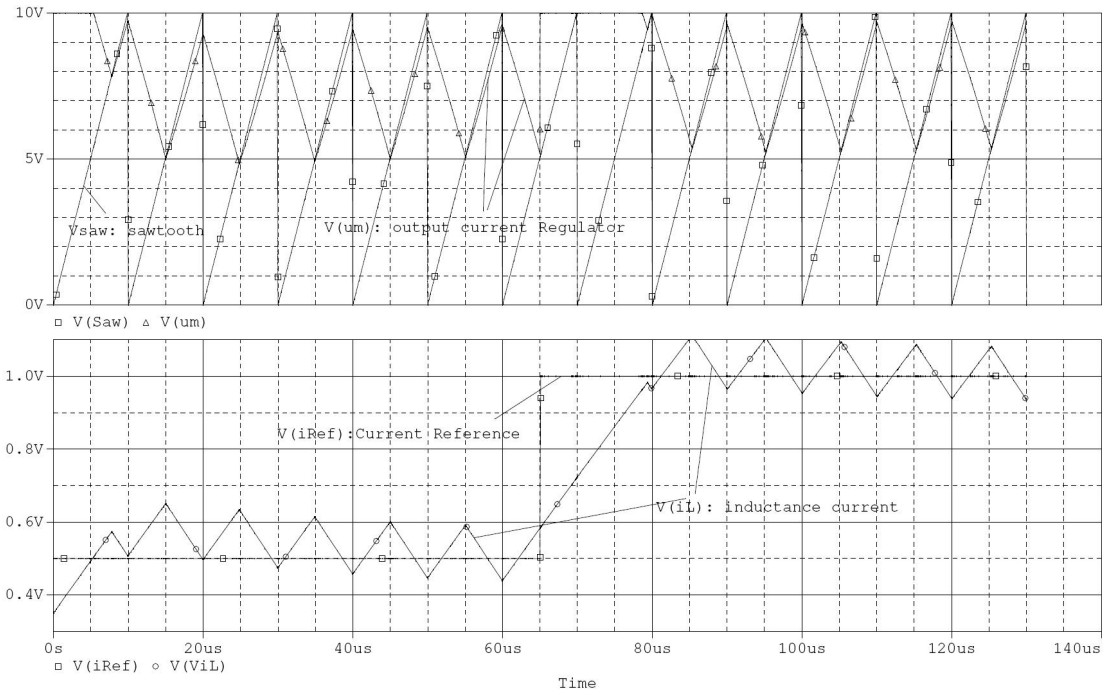

Figure 67: Results of the simulation of the circuit in figure 66.
V(iRef) represent the current reference;
V(viL) the voltage proportional to the current through the inductance;
V(saw) the oscillating voltage signal at the output of the sawtooth generator;
V(um) the output compensator signal.
Should be noticed that the upslope of the V(um) is equal to the upslope of the V(saw),because of the optimal choice of K_P.

gain:10^6; followed by a soft limiter, in order to reduce convergence problems in PSpice). The PWM block is composed as well by an ideal operational amplifier, as just described. The outside signal will command the switch.

As depicted in figure 67, the output compensator signal upslope is equal to the oscillator ramp slope, as consequence of the optimum K_P choice. Imposing the zero at $\omega_z = 3 \times 10^4$ rad/s, it is obtained K_I from relation $\omega_z = \frac{K_I}{K_p}$, results in $K_I = 9 \times 10^5$ V/s.

Calculation of K_I

Assuming a compensation network as depicted in figure 68, the values of the components can be calculated as in (4.31), choosing a value of $R_2 = 30$ kΩ; $K_P = \frac{R_2}{R_1} \rightarrow R_1 = 1$ kΩ and then
$\omega_z = \frac{1}{R_2 C_2} \rightarrow C_2 = 1$nF

$$G_{ri}(s) = \frac{1 + sR_2C_2}{sR_1C_2} \tag{4.31}$$

The PI compensation network is built as depicted in figure 68; choosing a value of $R_1 = 10$kΩ $R_2 = 30$kΩ and $C_2 = 1$nF.

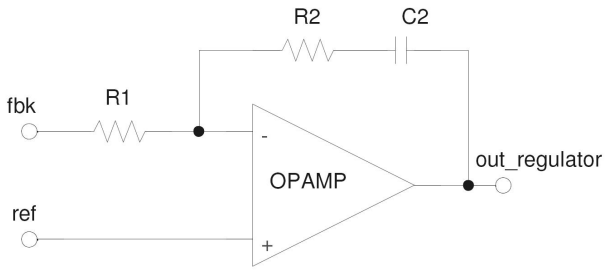

Figure 68: Regulator schematics

4.5 VOLTAGE EQUALIZATON CONTROL

In order to equalize the voltage between the batteries it is needed to inject a current into the weak battery. Beeing disconnected to the load, the voltage provide the state of charge (SOC) of the battery. For this reason the inner current loop must be controlled by an outside loop based on the comparison between the voltages of the batteries. A block scheme that resume the system is depicted in figure (69). It can be noticed that the current reference is decided by the outside-loop regulator. The input signal of this regulator is the difference between the voltage of the most charged battery and the weak one. $G_{u_o\delta}$ represent the transfer function between the control (δ) and the output voltage (u_o); G_{Ru} is instead the transfer function of the voltage loop regulator. Supposing that the current loop is fast enough, than it is possible assume no variations on i_L. Afterward, the inductance can be substituted by a current source ([40] pag.8-23). In order to design the compensation network, it is necessary find the transfer function between the reference signal and the output voltage $G_{u_cu_o}(s)$. In order to accomplish to this aim, a current source driven by an oscillating source is substituted to the inductance; and the bode plot resulting is showed in figure 70.

Transfer Function $G_{u_o\delta}$

Transfer function G_{R_u}

Transfer function $G_{u_cu_o}$

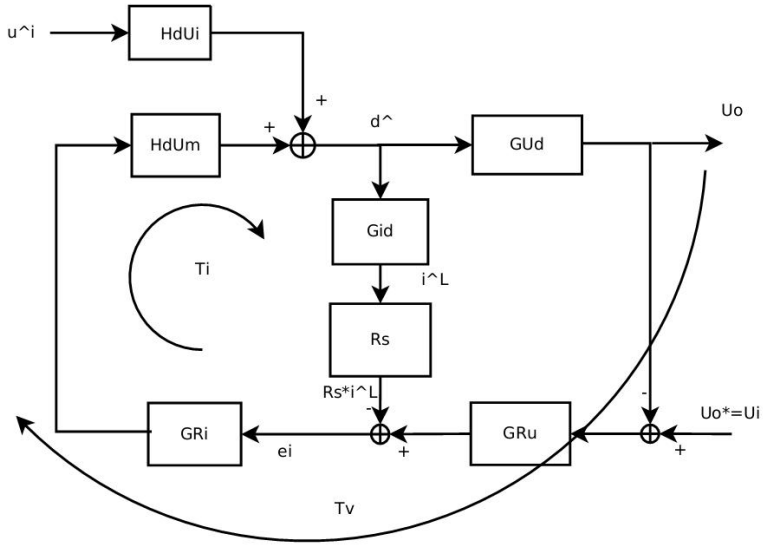

Figure 69: Block scheme

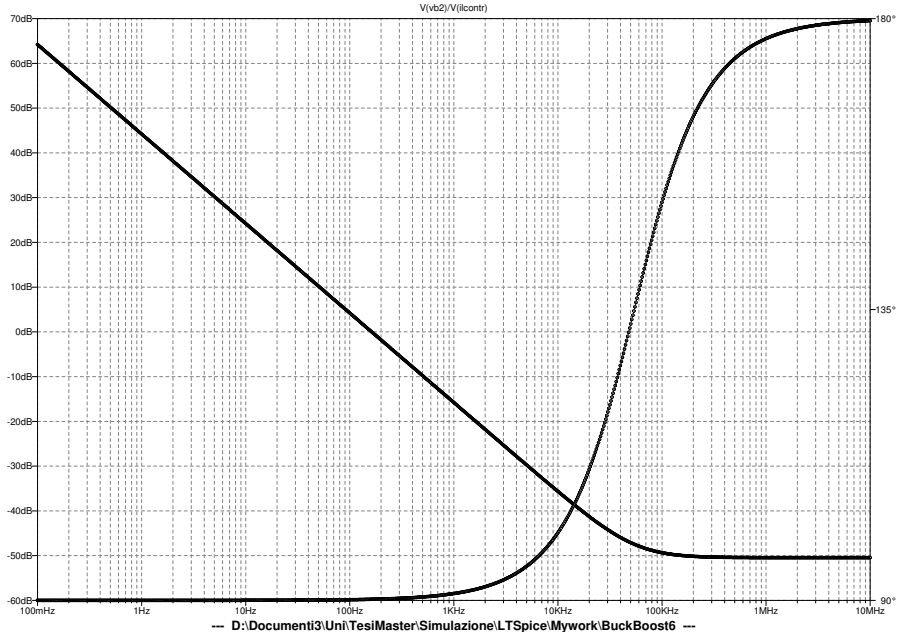

Figure 70: Transfer function $G_{u_c u_o}$ calculated with LTSpice though the average switching cell model

Being the $G_{u_c u_o}$ a transfer function with bandwidth 158 Hz, that means $\omega = 10^3$ rad/s, the regulator network is composed by an Op-Amp with odB gain as showed in figure 71. The resulting static curves depicted in figure **??** represent the voltages of the batteries that have to be equalized, at different duty cycle values (60%, 50%, 40%) the arrow indicate a decreasing value of Duty cycle.

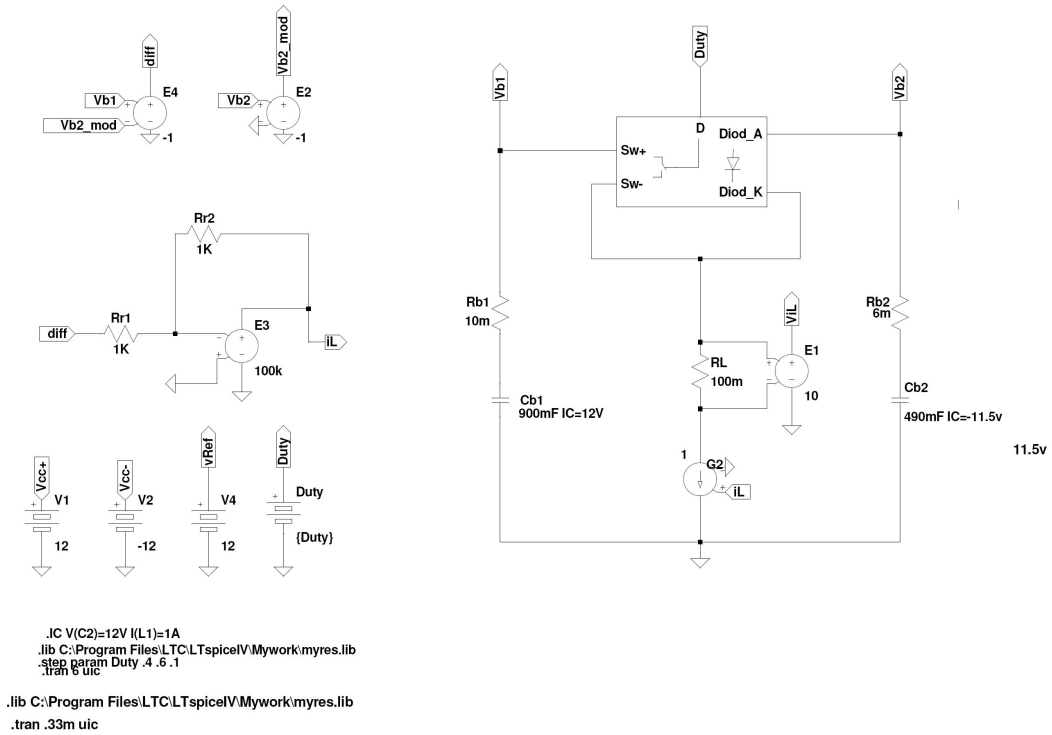

Figure 71: Circuit used to test the voltage regulator.

4.5.1 *Average switching cell method*

In the above discussion it is used an average model of the switching cell of the converter. The average model, as suggested in ([39] pag816); the following relations are true if averaged in the switching period:

$$v_{12}(t) = \frac{1-\delta(t)}{\delta(t)} \cdot v_{34}(t) \tag{4.32}$$

$$i_3(t) = \frac{1-\delta(t)}{\delta(t)} \cdot i_1(t) \tag{4.33}$$

$$\tag{4.34}$$

This model is presented in figure 73, and the code is provide hier in figure 73

The following LTSpice code constitute the average model of the "Switching cell" in CCM operating mode.

```
*********************************
*Subcircuit Average model switching cell -CCM mode
*********************************
```

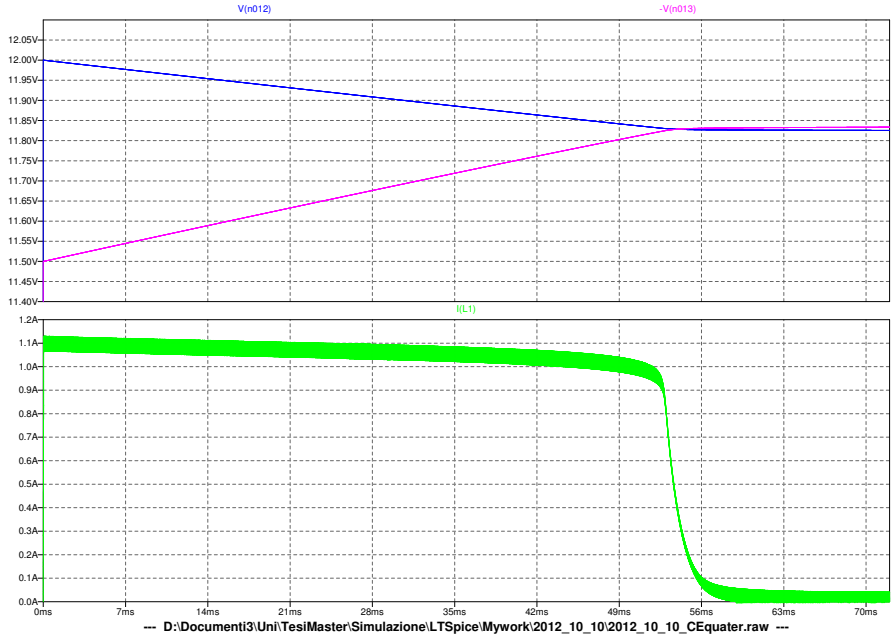

Figure 72: Battery voltages (on top of the figure) and current applied to the weakest battery; It can be notice that the voltage of the less charged battery rise up, and the most charged battery slow down to a common voltage value

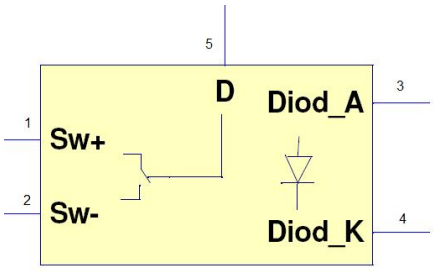

Figure 73: Average model of the switching cell CCM mode

```
Nodes:
*1: Transistor positive
*2: Transistor  negative
*3:diode cathode
*4:diode anode
*3:Duty cycle command
*****************************
.subckt myres 1 2 3 4 5
Et 1 2 value={(1-v(5))*v(3,4)/v(5)}
Gd 4 3 value={(1-v(5))*i(Et)/v(5)}
.ends myres
*******************************
```

Figure 74 shows that the waveform obtained by simulation of the averaged model, and that one obtained by the switching circuit model are comparable.

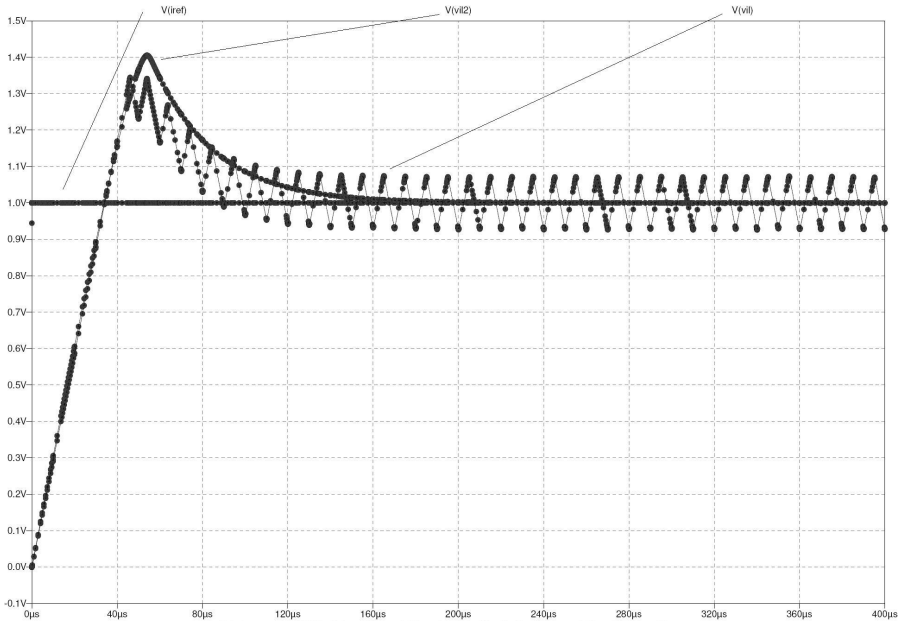

Figure 74: Current through the inductance simulated with the average switching cell model

CONCLUSIONS

A dual flyback topology used as Charge Equalizer is here analyzed. The aim was to build up a system that can provide galvanic insulation and doesn't use any capacitor. Capacitors are unwanted because those waste energy due to their parasitics losses. The system control is composed by an inner current loop and an outsider voltage loop. The current loop provides the charge from a battery to another, and the simple voltage loop has to equalize the voltage between the batteries. A design of the mutual inductor is also done, trying to optimize the design in order to get the maximal efficiency. A review of well-known charge equalizer are also presented, in order to understand which was could be the most efficient and fast method. Consequently the topology is chosen the topology. In the first part, an excursus over batteries and the way of determine the SOC and SOH was done. This gives evidence that in order to build up a voltage regulator, a predictive method is the best solution. In contrast to this, the empirical methods are not that kind of precise.

BIBLIOGRAPHY

[1] Technical Marketing Staff of Gates Energy Products, Inc., *"Rechargeable Batteries Applications Handbook"* c 1992 by Butterworth-Heinemann, a division of Reed Publishing (USA) Inc.ISBN 0-7506-9228-6

[2] T.M.Crompton; *"Battery reference book"* 3rd edition ;Newnes; ISBN 0-7506-4625

[3] Jian Cao; Nigel Schofield; Ali Emadi *"Battery balancing methods: a comprehensive review"*; vehicle power and propulsion conference, September 3-5, 2008, Harbin, China; IEEE 2008

[4] K.Cohl-Ho, M.Gun-Woo*"Charge equalizer method based on battery modularization"*; IEEE 2008

[5] S. Pang, J. Farrell, J. Du, and M. Barth; *"Battery state-of-charge estimation"* Proceedings of the American Control Conference, pp-1644-1649; Arlington, VA, June 25-27 2001

[6] B. Powell, T. Pilutti;*"Series Hybrid Dynamic Modeling and Control Law Synthesis"* Ford Scientific Research TR SR-93-201, December 1993.)

[7] Shinya Sato; Atsuo Kawamura; *"A New Estimation Method of State of Charge using Terminal Voltage and Internal Resistance for Lead Acid Battery"*; IEEE PCC OSAKA 2002

[8] Medora, N.K.; kusko, A.; *"Dynamic battery modeling of batteries using m unfacturers' data"*; telecommunications energy conference, 2006 INTELEC '06 28th Annual International Sept 2006 Pages 1-8

[9] Patrick J. van Bree, André Veltman, Will H. A. Hendrix, and Paul P. J. van den Bosch; *"Prediction of battery behaviour subject to hight-rate partial state of charge"*; Vehicular technology; IEEE transactions, Volume 58, Issue 2, Feb 2009 Pages 588-595

[10] Chalasani S C Bose, Doug Wilkins, Steve McCluer and Mike J.; *"Lessons learned in using ohmic techniques for battery monitoring"*; Proceedings of the 16th annual battery conference on applications and advances; IEEE; Gen 2001; Pgg 99-104

[11] Chih-Chiang Hua, Tzung-You Tasi, Chih-Wei Chuang, Wen-Bin Shr; *"Design and Implementation of a Residual Capacity Estimator for Lead-Acid Batteries"*; Industrial elecrtonics and appications, 2007, 2nd IEEE conference on 23-25 May 2007 Pages 2018-2023

[12] John Chiasson,Baskar Vairamohan; *Estimating the State of Charge of a Battery* IEEE

[13] S.T.Hung, D.Hopkins, C.R.Mosling *Extension of battery life via charge equalization control*; IEEE transactions on industrial electtronics, Vol.40, No 1, February 1993; Pages.96-104

[14] Mk batteries and american workschop; *"Sealed valve regulated (SVR) gelled electrolyte lead-acid batteries"*; Technical manual.

[15] Jian Cao; Nigel Schofield; Ali Emadi *"Battery Balancing Methods: a comprehensive review"*; vehicle power and propulsion conference, September 3-5, 2008, Harbin, China; IEEE 2008

[16] K.Cohl-Ho, M.Gun-Woo*"Charge equalizer method based on battery modularization"*; IEEE 2008

[17] N.H.Kutkut, D.M.Divan, D.W.Novotny; *"Charge equalization for series connected battery strings"*; IEEE 1995

[18] Pasqual switched capacitor *"Switched Capacitor System for automatic battery equalization"*; IEEE 1997

[19] H.Schmidt, C.Siedle; *"The Charge Equalizer - A new system to extend battery lifetime in PV-Systems, UPS and electric vehicles"*; Fraunhofer-Institut für solare energiesysteme; 12-16 October 1992

[20] C.Pascual, P.T.Krein; *"Switched Capacitor System for automatic battery equalization"*; IEEE 1997

[21] M.Tang, T.stuart; *"Selective Buck-Boost equalizer for series battery packs"*; IEEE transactions on aereospace mand electric systems Vol.36 No.1 January 2000 Pgg 201-210

[22] H.Leung *"Equalization of EV and HEV batteries with a ramp converter"*; IEEE transaction on aereospace and electronics systems Vol.3 No.1 January 1997 Pgg 307-312

[23] S.T.Hung, D.C.Hopkins, C.R.Mosling; *"Extension of battery life via charge equalization control"*; IEEE transaction Vol.40 No.1 February 1993 Pgg 96-104

[24] N. H. Kutkut, H.L.N. Wiegman, D.M. Divan,D.W.Novotny; *"Design Considerations for Charge Equalization of an Electric Vehicle Battery System"*; IEEE Transactions on Industry Applications, VOL. 35, NO. 1, January/february 1999

[25] Billings,K.;*"Switch mode power supply handbook"*-2nd Ed.; 1999 McGraw Hills; ISBN 0-07-006719-8

[26] *"Inductor and Flyback-Transformer Design"* Texas Application Notes http://focus.ti.com/lit/ml/slup127.pdf

[27] Lloyd H.Dixon *"Eddy current losses in transformer windings and Circuit wiring"*

[28] *"Data sheet Epcos"*

[29] *"Catalog Siemens-Matsuschita"*

[30] *"EF coil formers Type E20/10/6"* Epcos

[31] *"Application Notes Epcos"*

[32] J.Adams *"Flyback Transformer Design for the IRIS40xx series" Application Note AN-1024a ; IRQ-International Rectifier*

[33] *"Magnetic core for switching power supply"* Magnetics division of Spang and company

[34] http://www.harkis.harting.com/WebHelp/EGds/WebHelp/GBgdsCreepage_and_clearance_distances.htm

[35] T.M.Crompton; *"Battery referencee book"* 3rd edition ;Newnes; ISBN 0-7506-4625

[36] *"Application Notes Magnetics"*

[37] J.Sun, D.M.Mitchell *"Averaged Modeling of PWM converters operating in discontinious conduction mode"* IEEE transaction on power electronics, Vol 16 No4 July 2001;

[38] Lloyd Dixon; *" Average Current mode control of switching power supplies"*; Unitrode Application Note

[39] R.W.Erickson, D.Maksimovic, *"Fondamentals of power electronics"* second edition , Kluwer academic publishers, Massachusset, year 2001

[40] G.Spiazzi; *"Appunti dalle lezioni di elettronica di potenza"*, Libreria Progetto, 2006